Applied Catalysis B: Environmental 301 (2022) 120800

Contents lists available at ScienceDirect

Applied Catalysis B: Environmental

journal homepage: www.elsevier.com/locate/apcatb

Selective tandem catalysis for the synthesis of 5-hydroxymethylfurfural from glucose over in-situ phosphated titania catalysts: Insights into structure, bi-functionality and performance in flow microreactors

Wenze Guo [a], Thijn Kortenbach [a], Wei Qi [b], Emiel Hensen [c], Hero Jan Heeres [a], Jun Yue [a,*]

[a] Department of Chemical Engineering, Engineering and Technology Institute Groningen, University of Groningen, 9747 AG Groningen, the Netherlands
[b] Guangzhou Institute of Energy Conversion, Chinese Academy of Sciences, CAS Key Laboratory of Renewable Energy, No. 2 Nengyuan Road, Guangzhou 510640, China
[c] Department of Chemical Engineering and Chemistry, Eindhoven University of Technology, 5600 MB Eindhoven, the Netherlands

ARTICLE INFO

Keywords:
5-Hydroxymethylfurfural
Glucose
Phosphated titania
Solid acid
Microreactor

ABSTRACT

5-Hydroxymethylfurfural (HMF) synthesis from glucose over in-situ phosphated titania catalysts is presented. Phosphates were incorporated into titania framework forming a titanium phosphate surface layer, where the coordinatively unsaturated tetrahedral TiO_4 units act as water-tolerant Lewis acid site (LAS) and the adjacent protonated phosphate as Brønsted acid site (BAS), together forming Lewis-Brønsted acid pairs at molecular-level proximity. Glucose turnover and HMF selectivity were enhanced due to the rapid fructose transfer from LAS to the adjacent BAS for its dehydration to HMF, facilitating LAS liberation for another glucose turnover. Reactions in a water-2-methyltetrahydrofuran biphasic system in packed-bed microreactors gave 66% HMF yield (from 1 M glucose at 150 °C), where the HMF space time yield is about two orders of magnitude higher than that in batch and the literature work. Phosphate leaching from the catalyst is rather limited, whereas the catalyst deactivated mainly by humin deposition and could be regenerated by calcination.

1. Introduction

Use of biomass as a green and renewable alternative to conventional fossil feedstocks holds great promises towards developing a sustainable chemical industry in the near future. Herein, the transformation of lignocellulose into versatile platform chemicals represents an important approach [1,2]. Currently, high attention is given to the development of efficient catalytic systems and process technologies for the conversion of cellulosic carbohydrates into 5-hydroxylmethylfurfural (HMF), a key building block for various high value-added fine chemicals, biofuels and polymers [3]. One important application of HMF is in its oxidation to 2, 5-furandicarboxylic acid, which serves as the monomer of polyethylene furanoate (PEF), a promising replacement for conventional petroleum-based polyethylene terephthalate (PET) [4]. HMF can also be reduced via selective hydrogenation to 2,5-dimethylfuran and 2-methylfuran (promising liquid transportation fuels) [5]. Moreover, the rehydration of HMF produces levulinic acid which can be hydrogenated to γ-valerolactone (a non-toxic green solvent and promising fuel additive) [6].

HMF is typically produced by the dehydration of cellulosic C6 monosaccharides such as glucose and fructose, among which glucose is more attractive owing to its lower cost and highest abundance in nature [7]. However, the direct conversion of glucose to HMF is more difficult with a by far lower HMF selectivity compared with fructose [8]. Thus, glucose isomerization (over Lewis acid catalysts) to fructose, followed by fructose dehydration (over Brønsted acid catalysts) to HMF, has been extensively investigated and proven to be an effective pathway [3]. Homogeneous catalytic systems containing Lewis acids (e.g., mineral salts of Al(III), Cr(III), Zn(II) and Sn(IV)), with or without Brønsted acids (e.g., HCl, H_2SO_4 and H_3PO_4), have been widely reported active for glucose conversion to HMF [9–13]. Nevertheless, heterogeneous catalysts are preferred over homogeneous ones in the industrial production due to the ease of catalyst separation and reuse as well as less environmental pollution issues. Nowadays, numerous researches have been reported using zeolites, metal oxides/phosphates, ion exchange resins, heteropoly acids, modified carbon or their combinations as solid Lewis or/and Brønsted acid catalysts for glucose conversion to HMF. Most efforts therein have been made on regulating the relative abundance and strength of Lewis acid site (LAS) and Brønsted acid site (BAS) to improve their cooperativity for HMF synthesis [14,15]. It is noteworthy that HMF

* Corresponding author.
E-mail address: Yue.Jun@rug.nl (J. Yue).

https://doi.org/10.1016/j.apcatb.2021.120800
Received 9 August 2021; Received in revised form 4 October 2021; Accepted 5 October 2021
Available online 8 October 2021

synthesis over such solid catalysts was often studied in a non-aqueous reaction medium (e.g., ionic liquids and polar aprotic solvents) [13,14,16–22], due to the considerations of (*i*) the deactivation of LAS by its hydration in water on catalysts such as silicoaluminate zeolites [23,24]; (*ii*) the leaching of active sites like sulfate and phosphate on the anion-modified solid acid catalysts into water under hydrothermal reaction conditions (e.g., >150 °C) [25,26]; (*iii*) a better chemistry in ionic liquids or organic solvents (e.g., DMSO) with less formation of byproducts such as formic acid, levulinic acid and humins [3]. However, high expense of ionic liquids and difficulty in the downstream separation of HMF from organic solvents with high boiling points are significant drawbacks for their industrial uses. Moreover, the glucose feed stream in bio-refinery is mostly in the form of aqueous solution (e.g., obtained from hydrolysis of starch or cellulose) [27]. Therefore, water as a green and cheap solvent is a better choice for HMF production from glucose. To suppress HMF-involved side reactions in water, the concept of utilizing an aqueous-organic biphasic system has been proven useful, as the majority of HMF formed in the aqueous medium could be extracted into the (non-reactive) organic phase during the reaction [28]. Consequently, water-tolerant solid acid catalysts for efficient HMF synthesis from glucose in biphasic systems are highly demanded and have received significant research attention [14,29].

A typically low-cost and ecofriendly solid acid catalyst is anatase titania which is well known for its rich surface chemistry and chemical stability [30,31]. Anatase is considered a water-tolerant Lewis acid catalyst, due to the presence of unsaturated tetrahedral TiO_4 with mild Lewis acidity preventing hydration in water [31–34]. Brønsted acidity could be further introduced into titania by modification with anions such as sulfate, phosphate and tungstate [35–38]. Particularly, phosphated titania (P-TiO_2) has been reported to be highly effective for HMF synthesis from glucose [33–36]. By far, most reported P-TiO_2 catalysts for glucose conversion were synthesized by post-phosphation methods. For instance, Atanda et al. [35,36] prepared P-TiO_2 by impregnating titanium hydroxide with ammonium phosphate. Phosphates were found to promote Brønsted acidity at the expense of Lewis acidity, and a promising HMF yield of 63% from 5 wt% glucose was obtained at 175 °C in 105 min in a biphasic water-tetrahydrofuran (THF) system. Hara and co-workers [33,34] prepared P-TiO_2 by simply treating anatase with concentrated phosphoric acid. Phosphates were anchored onto the titania surface by esterification between the surface Ti-OH and H_3PO_4 forming Ti-O-$PO(OH)_2$ (monodentate ligation). The catalyst acidity was found unchanged after phosphation (i.e., having the same amount of LAS as the parent titania without Brønsted acidity), whereas the HMF selectivity from glucose in the aqueous THF solution was largely improved from 8.5% (over the parent titania) to 81.2% (over P-TiO_2) at 120 °C in 2 h, indicating a reaction mechanism beyond acid catalysis. Interestingly, via an isotopically labeled method they found that glucose conversion over LAS underwent a direct dehydration pathway with 3-deoxyglucosone as an intermediate, rather than the typical tandem glucose isomerization-fructose dehydration route [33]. This pathway was subsequently rationalized (via a density functional theory simulation) by a synergistic effect between Lewis acidic Ti sites and the vicinal basic oxygen sites of Ti-OH group [39]. However, the promoting effect of phosphates in their case still remains unclear. The above results show that the structure, acidic property and catalytic performance of P-TiO_2 catalysts related to HMF synthesis from glucose (in aqueous reaction media) strongly depend on the synthesis method, where the underlying relationship between these remains not well elucidated yet and thus is one aim of this work. Notably, by the post-phosphation methods, phosphates usually exist as surface species anchored to the titania phase, which is often unstable and tends to leach under hydrothermal reaction conditions, causing irreversible catalyst deactivation [25]. Moreover, these surface structures usually lead to irregular proximity between LAS and BAS, which has been rarely studied, but has shown a great importance in the tandem catalysis for glucose conversion [40]. In addition, the reported P-TiO_2 catalysts often exhibit low surface areas (< 200 m^2/g) and limited internal porosity [35,36,41–45], which tend to restrict not only the amount and accessibility of surface acid sites, but also their further incorporation into continuous flow reactor setup as a packed bed because of high pressure drop penalty. Thus, an improved synthesis method is needed for P-TiO_2 catalysts with better textural properties, hydrothermal stability and optimized LAS-BAS proximity and cooperativity.

HMF synthesis in batch reactors is well-documented, but its continuous production (particularly from glucose over heterogeneous catalysts) has been much less reported [46]. Atanda et al. [36] investigated the conversion of soluble cello-oligomers over the post-phosphated titania catalyst in a continuous flow packed-bed reactor. An HMF yield of 53% was obtained at 220 °C and a liquid hourly space velocity of 18.9 h^{-1} in the water-methylisobutylketone (MIBK) biphasic system. However, a decreased HMF yield was observed after 1 h time-on-stream, while the leaching of phosphate as a possible cause and catalyst regeneration were not studied. Generally, the catalyst stability and reusability are of great importance for scaled-up HMF production especially in continuous processing. In most researches the stability evaluation was conducted batch-wise at a high glucose conversion. This does not allow for an accurate assessment and the possibility that the reaction promoted by the leached homogeneous acid is difficult to exclude [47]. Consequently, it is necessary to study P-TiO_2 catalysts in a flow reactor not only to increase the space time yield of HMF, but also to more accurately assess the catalyst stability, as well as to understand the causes and rates of deactivation for consideration in the following catalyst regeneration. Compared with conventional batch reactors, continuous flow microreactors with packed catalyst bed have certain advantages such as much higher heat and mass transfer rates [46,48] and thus represent a promising tool for reaction study or production unit. In the past years, microreactors have been used for the synthesis of HMF or 5-chloromethylfurfural (CMF) from fructose or glucose in a single or biphasic solvent system with homogeneous catalysts [8,9,49–55]. However, the combination of heterogeneous catalyst for glucose conversion to HMF and flow processing in a biphasic system in microreactors has not been explored yet [46,48].

Herein, we present an in-situ phosphation approach for the synthesis of P-TiO_2, aiming to incorporate phosphates into the titania framework forming a robust structure against hydrothermal leaching, and to achieve a regular and close proximity between LAS and BAS. The physiochemical properties of P-TiO_2 catalysts were characterized systematically and their performance was firstly investigated in batch using a water-2-methyltetrahydrofuran (mTHF; a green biobased solvent) biphasic system, where further catalyst modification by ion exchange and silylation was used to study the role of surface LAS and BAS in glucose conversion. The effect of proximity between LAS and BAS was studied by a performance comparison between the in-situ P-TiO_2 and physically combined Lewis and Brønsted acid catalysts. The relation between the structure, surface acidity and bi-functionality of the in-situ P-TiO_2 catalyst was then elucidated. Subsequently, the catalyst was loaded into a microreactor as packed bed to study the flow reaction characteristics and catalyst deactivation behavior. The catalytic performance in batch and flow was compared with the literature work and future microreactor optimization strategy was discussed.

2. Experimental section

2.1. Materials

D-glucose (99 wt%), D-fructose (99 wt%), D-mannose (99 wt%), mTHF (99 wt%) were purchased from Acros Organics Co., Ltd. HMF (99 wt%), formic acid (99 wt%), levulinic acid (99 wt%), anhydrous ethanol (99.5 wt%), Pluronic P123 (99 wt%; molecular weight: 5800 g/mol), phosphoric acid (85 wt%), nitric acid (65 wt%), sodium carbonate (99.5 wt%), titanium butoxide (99 wt%), sodium chloride (99 wt%) and tetraethyl orthosilicate (99 wt%) were all purchased from Sigma-Aldrich

Co., Ltd. Amberlyst-16 resins (acidity: 4.80 mmol H^+/g) were supplied by DuPont Company. All chemicals were of chemical grade and used as received without further treatment. MiliQ water was used through all the experiments. Ace pressure glass tubes (height of 10.2 cm; outer diameter of 19 mm; volume of 9 mL) were used as the laboratory batch reactor and supplied by Sigma-Aldrich Co., Ltd. Perfluoroalkoxy alkane (PFA) tubings (inner diameter: 4 mm) were used as microreactors and supplied by CBN company.

2.2. Synthesis and regeneration of the in-situ phosphated titania catalyst

The in-situ phosphated titania catalyst (P-TiO_2) was synthesized using a simple one-pot sol-gel method, with a low temperature (ca. 0 °C) to mitigate the fast hydrolysis and condensation of titanium butoxide, and allow a gentle and controllable sol-gel process. In detail, 4.35 g of P123 was dissolved in 38 g of anhydrous ethanol and stirred at room temperature for 1 h to get a transparent solution A. Then, 10.2 g of titanium butoxide (99 wt%) and 0.89 g of HNO_3 (65 wt%) were added into the former solution A and stirred in an ice bath for 1 h. In another container, a certain amount of H_3PO_4 was dissolved in 3.24 g of anhydrous ethanol and 3.24 g water, and the formed solution B was added dropwise into the above-mentioned solution A under vigorous stirring. The resulting solution was further stirred in the ice bath for another 1 h, and then kept static at room temperature. After aging for 24 h, a white gel was formed, which was then subjected to slow and thorough evaporation at 60 °C in an oven for 24 h. The dried gel obtained was calcined at 400 °C for 6 h with a heating rate of 2 °C/min to remove the organic template and obtain the in-situ P-TiO_2 catalyst. As a reference, pure titania was synthesized by the same procedure above, but without the addition of H_3PO_4. The catalysts synthesized by the above procedure were named as *X* P-TiO_2, where *X* denotes the molar ratio of P to Ti.

After the reaction test (in microreactors), the used P-TiO_2 catalysts were regenerated by washing with water and ethanol followed by drying at 60 °C for 2 h and calcination in air at 400 °C for 6 h.

2.3. Modification of the in-situ phosphated titania catalyst

Silylation has been reported as an effective method to selectively deactivate the isolated LAS in the zirconium phosphate catalyst with little effect on paired LAS and BAS [40,56]. Similarly, 0.05 P-TiO_2 was silylated using tetraethyl orthosilicate (TEOS) to reduce the extra isolated LAS according to the literature [40]. 1 g of 0.05 P-TiO_2 catalyst was added to a solution of 0.25 g TEOS in 20 mL n-hexane. The mixture was stirred at 50 °C for 24 h, followed by washing with ethanol and water, and finally drying at 60 °C for 24 h.

To eliminate BAS, sodium exchanged 0.10 P-TiO_2 was prepared according to the literature [40], by mixing 1 g of 0.10 P-TiO_2 catalyst with 20 mL aqueous solution of 1 M sodium carbonate under stirring at 50 °C for 24 h, followed by washing with water and drying at 60 °C for 24 h.

2.4. Catalyst characterization

Inductively coupled plasma atomic emission spectroscopy (ICP-AES) was conducted on Optima 7000 DV Optical Emission Spectrometer (PerkinElmer, USA). Powder X-ray diffraction (XRD) analyses were performed on a D8 Advance Powder Diffractometer (Bruker, Germany) using Cu Kα emission radiation (λ = 1.5418 Å) operated at 40 kV and 40 mA with a LYNXEYE detector (1D mode). Fourier transform infrared (FTIR) spectra were recorded on an IRTracer-100 FT-IR spectrophotometer at a resolution of 4 cm^{-1} with wavenumber range of 600–4000 cm^{-1}. Nitrogen adsorption-desorption isotherms were obtained at 77 K on ASAP 2420 Surface Area and Porosity Analyzer (Micromeritics, USA). Samples were degassed at 120 °C for 12 h prior to the measurement. TEM images were taken on Tecnai T20 transmission electron microscope (FEI, NL) equipped with Gatan 2k×2k CCD camera. The samples were grinded and dispersed ultrasonically in ethanol and deposited on a carbon-coated copper grid prior to the measurement. SEM images were taken on a PHILIPS/FEI XL30 FEG scanning electron microscope equipped with energy dispersive X-ray spectrometer (EDX) Noran 6 system. X-ray photoelectron spectroscopy (XPS) measurements were conducted on a Thermo Scientific K-Alpha, equipped with a monochromatic small-spot X-ray source and a 180° double focusing hemispherical analyzer with a 128-channel detector. Data analysis was conducted using CasaXPS software. NH_3-TPD measurements were performed on AutoChem-II (Micromeritic, USA) equipped with a thermal conductivity detector (TCD). The catalyst was pretreated at 600 °C for 1 h before saturation with NH_3 and heating to 600 °C at 10 °C min^{-1}. Pyridine-IR spectra were recorded on a Nicolet 6700 FT-IR spectrometer (Thermo Fisher Scientific, USA) with a home-made cell connected to a vacuum-adsorption device. Samples were evacuated at 150, 250 or 350 °C before recording the IR spectra of adsorbed pyridine to study the strength of acid sites. The BAS and LAS were quantified by Lambert-Beer law based on extinction coefficients for bands at 1540 and 1446 cm^{-1}, respectively.

2.5. Glucose conversion to HMF

2.5.1. Batch reactor study

Performance of the in-situ P-TiO_2 catalyst for glucose conversion to HMF was firstly studied in the batch reactor. The prepared solid catalyst was pulverized and used in the form of 25–75 μm powders. In a typical run, 0.018 g of the catalyst, 1 mL of the aqueous solution containing 0.1 M glucose and 20 wt% NaCl (to promote HMF partition into mTHF), and 4 mL of mTHF were added into the pressure tube, followed by being sealed and heated at a certain temperature for a certain time under magnetic stirring at 600 rpm in an oil bath. The actual temperature was monitored with a calibrated thermocouple inserted into the reactor. The time when the reactor was immerged into the oil bath was considered as the starting point. At the end of the reaction, the tube was quenched in cooled water (at ca. 20 °C). The aqueous and organic phases were filtered through a polytetrafluoroethylene (PTFE, 0.45 μm) filter before their analysis by high performance liquid chromatography (HPLC) and gas chromatography (GC), respectively. The same procedure also applied for experiments with other substrates (fructose or HMF). The experiments under representative conditions were conducted at least twice, where a good reproducibility was usually obtained with a standard deviation of the results within 5%.

To get insights into the HMF partition between water and mTHF, the partition coefficient of HMF was measured under reaction conditions (150 °C, 0.1 M HMF, 1 mL water and 4 mL mTHF, with or without 20 wt % of NaCl) according to the procedure reported in our previous work [8] (cf. more details in Section S2.2 of the Supplementary Material).

2.5.2. Packed-bed microreactor study

The present P-TiO_2 catalyst powder was further tableted and pulverized to 300–425 μm before loading into the PFA microreactor as packed bed, as shown in Fig. 1. Typically, the aqueous feed is glucose solution containing 20 wt% NaCl, and the organic feed mTHF. Both phases were fed to the microreactor using a binary HPLC pump unit (Agilent 1200 Series) at an inlet organic to aqueous volumetric flow ratio (Q_{org}/Q_{aq}) of 4:1. The two phases were mixed in a polyether ether ketone (PEEK) Y-connector (inner diameter: 1.65 mm) to generate a uniform slug flow before reaching the packed bed. The mass of catalyst bed is typically 1.3 g (corresponding to a length of ca. 4 cm), except for some additional experiments to study the effect of catalyst loading where packed beds of 0.6 g and 2.6 g were also used. The packed-bed microreactor was placed vertically in an oven at 150 °C. A 50 μm inline filter (stainless steel) was connected to the bottom of catalyst bed. The top product mixture from the packed bed then flowed out of the oven through an empty capillary section of the microreactor which further passed through a water bath (ca. 20 °C) to quench the reaction. A back pressure regulator was installed at the end of the microreactor to

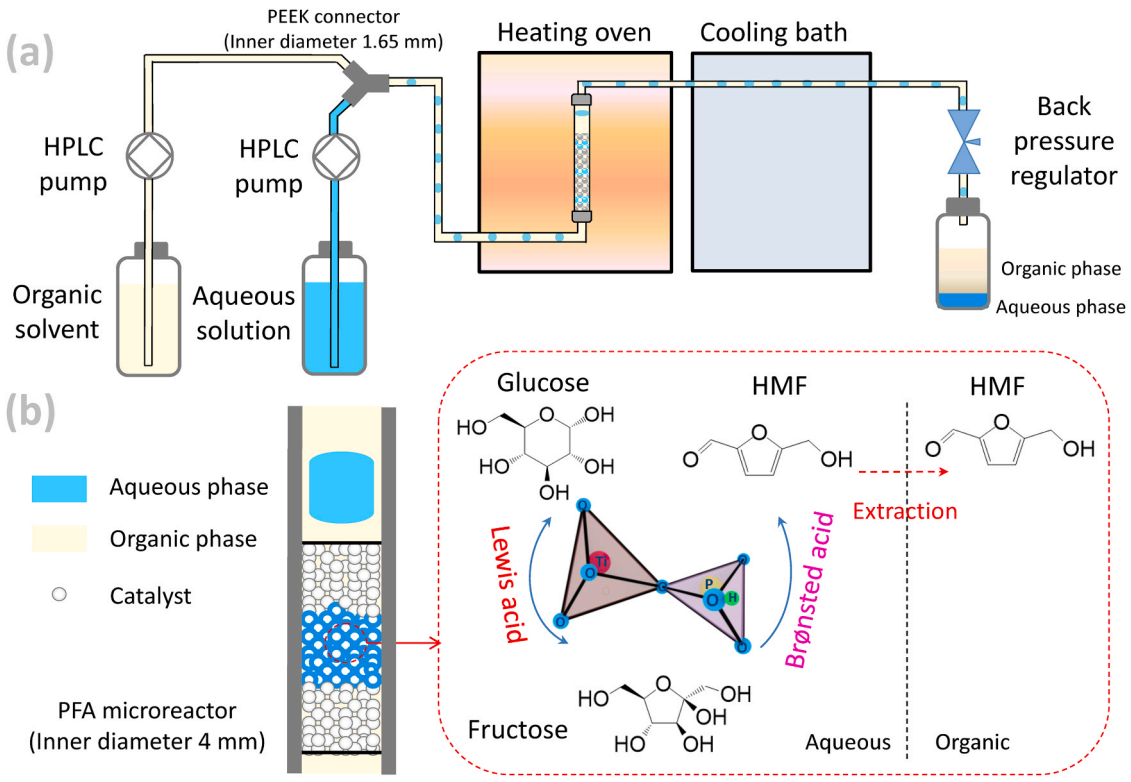

Fig. 1. Schematic representation of (a) the microreactor setup for HMF synthesis from glucose over the packed P-TiO_2 catalyst and (b) the plausible flow pattern (containing mainly fine organic droplets in the continuous aqueous phase) through the catalyst bed and tandem catalysis over Lewis-Brønsted acid pairs on the present P-TiO_2 catalyst with HMF being extracted from the aqueous to organic phase.

maintain a constant pressure of around 10 bar to ensure a liquid state of the content. The collected aqueous and organic phases were filtered before their analysis by HPLC and GC, respectively. The weight hourly space velocity (*WHSV*) in the microreactor was varied by adjusting the phasic flow rate.

2.6. Analysis, definitions and calculations

The composition of aqueous phase was analyzed by an Agilent 1200 HPLC, equipped with an Agilent 1200 pump, a refractive index detector, a standard ultraviolet detector as well as a Bio-Rad organic acid column (Aminex HPX-87H). A diluted aqueous H_2SO_4 solution (5 mM, 0.55 mL/min) was used as the eluent, and the temperature of the column was maintained at 60 °C. The analysis was complete within 60 min. The organic phase was analyzed by a TraceGC ultra GC, equipped with a flame ionization detector and a fused silica column (Stabilwax-DA). The concentrations of components in the aqueous and organic samples were determined from calibration curves obtained using the standard solutions with known concentrations.

In the batch reactor, the conversion of substrate *i* (X_i) and yield of product *j* (Y_j) are defined by Eqs. 1 and 2.

$$X_i = \frac{C_{aq,i,0} - C_{aq,i,1}}{C_{aq,i,0}} \times 100\% \quad (1)$$

$$Y_j = \frac{V_{org} C_{org,j,1} + V_{aq} C_{aq,j,1}}{V_{aq} C_{aq,i,0}} \times 100\% \quad (2)$$

In the above equations, V_{aq} and V_{org} designate the volumes of aqueous and organic phases at the start of the reaction (at ca. 20 °C), respectively. Considering the partial miscibility of water and mTHF, the two phases were mixed and saturated with each other before the reaction. Therefore, the volume of two phases were considered unchanged at the end of the reaction (at ca. 20 °C). $C_{aq,i,0}$ and $C_{aq,i,1}$ refer to the concentrations of substrate *i* in the aqueous solutions at the start and end of the reaction, respectively. $C_{aq,j,1}$ and $C_{org,j,1}$ represent the concentration of product j in the aqueous and organic phases at the end of the reaction, respectively.

The initial reaction rate was roughly estimated during the first 20 min' batch time within which the substrate conversion was kept at a relatively low level (up to ca. 25%). Turnover frequency (TOF) values of glucose over LAS, and of fructose and HMF over BAS, were calculated by Eq. 3.

$$TOF = \frac{Total\ amount\ of\ the\ consumed\ substrate\ or\ formed\ product}{Batch\ time \times Total\ amount\ of\ Lewis\ or\ Brønsted\ acid\ sites} \quad (3)$$

Similarly, the conversion of substrate *i* (X_i) and the yield of product *j* (Y_j) in the microreactor are defined by Eqs. 1 and 4, respectively.

$$Y_j = \frac{Q_{org} C_{org,j,1} + Q_{aq} C_{aq,j,1}}{Q_{aq} C_{aq,i,0}} \times 100\% \quad (4)$$

where Q_{aq} and Q_{org} refer to the flow rates of aqueous and organic phases at the microreactor inlet (at ca. 20 °C), respectively, which are equal to the corresponding flow rates at the microreactor outlet (at ca. 20 °C).

The weight hourly space velocity of the liquid (*WHSV*) is defined as

$$WHSV = \frac{Q_{org} + Q_{aq}}{w_C} \quad (5)$$

where w_C is the catalyst weight.

The carbon balance is defined as

$$C\ balance = \frac{C\ amount\ in\ the\ product + C\ amount\ in\ the\ remaining\ substrate}{C\ amount\ in\ the\ starting\ substrate} \times 100\% \quad (6)$$

The carbon balance is based on the quantified products by HPLC and GC (including glucose, fructose, mannose, HMF, levulinic acid and formic acid). It does not account for the non-identified intermediates and soluble/insoluble byproducts (e.g., humins).

3. Results and discussion

3.1. Physiochemical properties of the in-situ phosphated titania catalyst

3.1.1. Crystalline, surface structure and textural properties

The crystalline structure of the in-situ P-TiO_2 catalysts with different P loadings was characterized by wide-angle XRD (Fig. 2a). Pure titania exhibits a typical anatase crystalline structure. After loading phosphate, the diffraction peaks characterizing anatase broadened and decreased in intensity with increasing P/Ti ratios up to 0.10, which is related to the decrease in anatase crystallite sizes and the more amorphous nature of titania phase in P-TiO_2 samples. At P/Ti ratios higher than 0.10, the peaks characterizing anatase totally disappeared and P-TiO_2 samples turned fully amorphous. This is consistent with literatures indicating that the addition of phosphates decreases the anatase crystallinity and increases the transformation temperature of anatase to rutile due to the growth inhibition of anatase crystallite [43–45,57–59]. Besides, the collapse of ordered mesoporous framework in pure titania is clearly revealed by the absence of peak in its low-angle XRD pattern (Fig. S1). This is caused by the sintering and growth of TiO_2 grains during the calcination [57,58], as reflected in its narrower diffraction peak (Fig. 2a). Comparatively, all P-TiO_2 samples exhibit one apparent diffraction peak in the low angle region (Fig. S1), indicating a regular mesoporous structure which is stabilized by phosphates during the calcination.

The inhibition of anatase crystallite growth and stabilization of the ordered mesoporosity are related to the structure of phosphate species in P-TiO_2 catalysts. Generally, the phosphate species was considered to be either attached to the titania surface forming monodentate ligation, bidentate ligation or polyphosphate (Scheme 1, structures I-III), or inserted into the titania framework forming titanium phosphate (Scheme 1, structure IV) [33–35,43–45,57–61]. Typically, phosphate in the post P-TiO_2 catalyst has been reported to exist as surface species [33–35,59,60]. To further understand the nature of phosphate species in the in-situ P-TiO_2 samples here, FTIR characterization was conducted (Fig. 3). The broad peaks at 3200 cm^{-1} and 1630 cm^{-1} correspond to the surface hydroxyl groups and adsorbed water, which are higher in intensity for P-TiO_2 than titania. The peaks at 645 and 820 cm^{-1} present for all samples correspond to the Ti-O stretching vibrations of octahedral TiO_6 units [62,63]. One strong band at 990–1030 cm^{-1}, observed for all P-TiO_2 samples (but absent in pure titania), is typically a characteristic of PO_4 group (i.e., attributed to the P-O stretching vibrations from the surface phosphate (PO_4^{3-}), polyphosphate, or phosphate inserted into titania framework; Scheme 1). However, another characteristic peak of PO_4^{3-}, the P═O (phosphoryl) group usually at 1300–1450 cm^{-1} [64–66] is absent for all P-TiO_2, indicating the absence of phosphate species in monodentate or bidentate ligation and polyphosphates on the surface. Besides, it was reported that the P-O-P bending vibration has a characteristic peak at around 635 cm^{-1} [62,63], while in our case no distinct peak appears before 640 cm^{-1} for P-TiO_2, further supporting the absence of polyphosphates. Consequently, phosphates are considered to be incorporated into the titania framework, possibly forming a new titanium phosphate phase (Scheme 1, structure IV).

Since no other diffraction peak was observed in the XRD pattern characterizing titanium phosphate crystallines (Fig. 2a), titanium phosphate is likely present in the amorphous nature. To support this hypothesis, the 0.15 P-TiO_2 sample was calcined at higher temperatures (500–800 °C) for 6 h, and characterized by wide angle XRD (Fig. 2b). The peaks of anatase titania, which are absent in the amorphous sample calcined at 400 °C, appeared and turned higher in intensity with increasing calcination temperature (which favors the crystallite growth). After calcination at 800 °C, additional peaks appeared and were identified as a new crystalline phase, titanium pyrophosphate TiP_2O_7 (JCPDS 38-1468). It is known that the surface phosphate species does not react with titania phase transforming into titanium phosphate regardless of calcination temperature [43,59]. Therefore, the results here confirmed the incorporation of phosphate into the titania framework forming an amorphous phase on the prepared catalyst.

The total and surface compositions (i.e., P to Ti molar ratios) of P-TiO_2 were determined by ICP and XPS, respectively (Table 1). The measured total P/Ti ratios agree well with the calculated values in the sample synthesis, suggesting the complete incorporation of the added phosphates into titania by this in-situ phosphation method. The surface P/Ti ratios are by far higher than the total P/Ti ratios (e.g., being respectively 0.14 and 0.044 for 0.05 P-TiO_2, and 0.28 and 0.146 for 0.15 P-TiO_2). This indicates that the formed titanium phosphate phase mainly accumulated on the surface region of P-TiO_2. In a reference

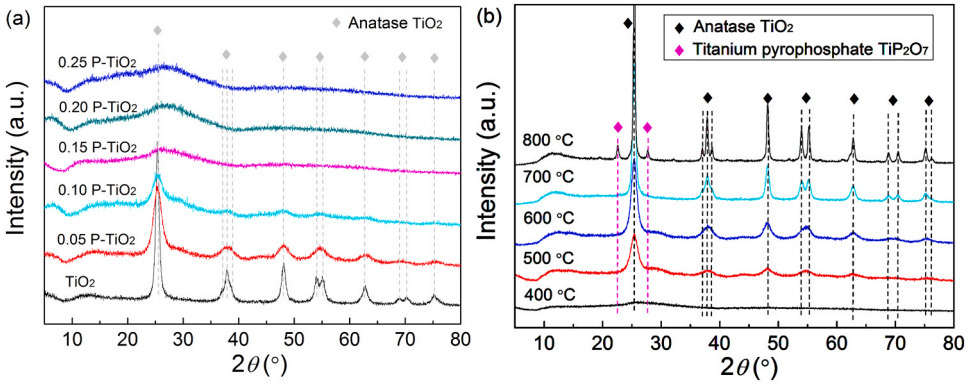

Fig. 2. Wide-angle powder XRD patterns of (a) P-TiO_2 catalysts with different P loadings calcined at 400 °C and (b) 0.15 P-TiO_2 catalysts calcined at different temperatures.

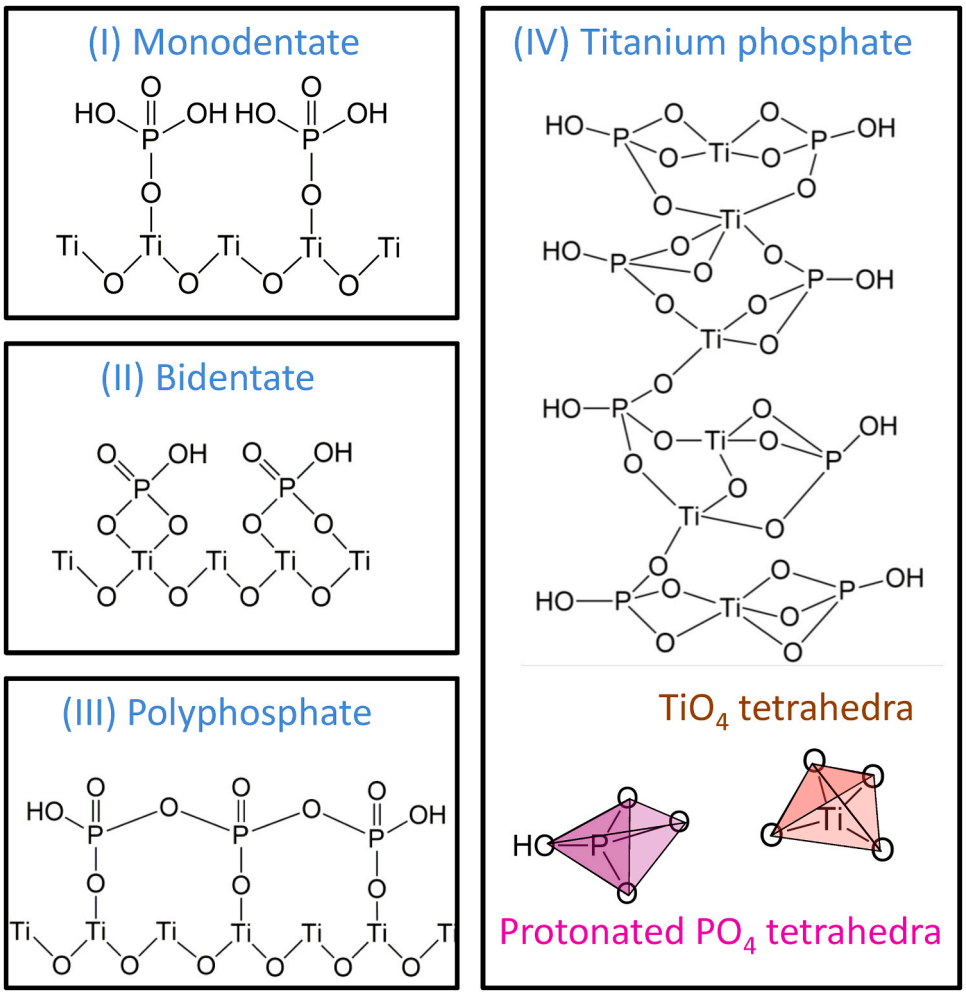

Scheme 1. Schematic representation of the surface structures of P-TiO_2.

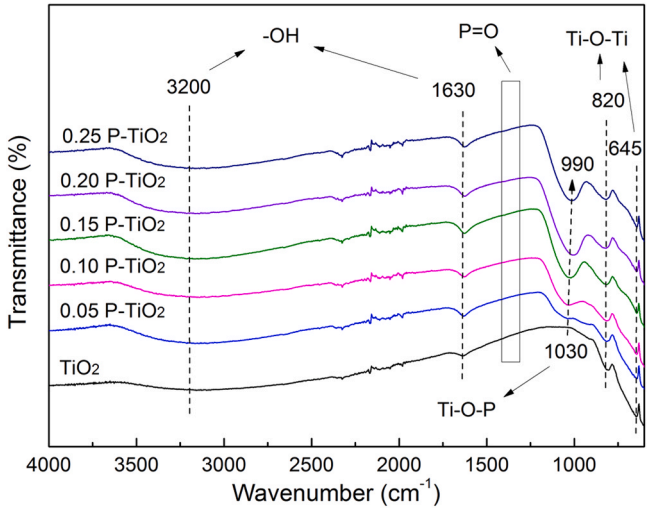

Fig. 3. FTIR spectra of the in-situ P-TiO_2 catalysts with different P loadings.

sample with a P/Ti ratio up to 0.5 (which refers more to titanium phosphate rather than phosphated titania catalyst), the surface P/Ti ratio was measured to be up to 0.88. This further suggests a generally increasing trend of surface P/Ti ratio with increased P loading in the prepared P-TiO_2 catalysts.

Table 1
Composition and textural properties of the in-situ P-TiO_2 catalyst.

Sample	P/Ti molar ratio		Surface area[c] (m^2/g)	Pore size[c] (nm)	Pore volume[c] (cm^3/g)
	Surface[a]	Total[b]			
TiO_2	0	0	135	3.6	0.17
0.05 P-TiO_2	0.14	0.044	225	3.0	0.21
0.10 P-TiO_2	n.d.[d]	0.099	262	2.9	0.23
0.15 P-TiO_2	0.28	0.146	307	3.0	0.28
0.20 P-TiO_2	n.d.[d]	0.199	287	3.0	0.27
0.25 P-TiO_2	n.d.[d]	0.248	285	3.1	0.27

[a] Determined by XPS.
[b] Determined by ICP.
[c] Determined by N_2 physisorption.
[d] Not determined.

The textural properties of the in-situ P-TiO_2 samples with various P loadings were characterized by N_2 physisorption (Fig. S2 and Table 1). According to IUPAC nomenclature, all samples exhibited a typical IV adsorption isotherm followed by H2 hysteresis loop (Fig. S2a), indicating the presence of ink bottle-shaped or cage-like mesoporosity. The average pore size of P-TiO_2 (ca. 3.0 nm) is lower than that of titania (3.6 nm) (Table 1). Besides, the narrower pore size distribution than that

of titania indicates the higher uniformity of mesopores in P-TiO_2 (Fig. S2b). The BET surface area of titania (135 m^2/g) is lower than (around) half that of P-TiO_2 samples (Table 1). With increased P loading, the catalyst surface area increased till a maximum of 307 m^2/g for 0.15 P-TiO_2, followed by a slight decrease afterwards for 0.20 and 0.25 P-TiO_2 (Table 1). Similar trends were also observed in the pore volume of P-TiO_2 samples. The in-situ P-TiO_2 catalyst here generally provides a higher surface area than the post P-TiO_2 in the literature (often <200 m^2/g) [35,36,43–45]. Compared with titania, the higher surface area and pore volume, and lower pore size of P-TiO_2 are attributed to the less sintering and higher mesoporosity (Fig. S1), as the formation of amorphous titanium phosphate phase acting as a diffusion barrier suppressed TiO_2 crystalline growth and grain sintering during the calcination. At the P/Ti ratio of about 0.15, the surface region of P-TiO_2 catalyst might already consist of titanium phosphate phase mainly, and thus the promoting effect on the inhibition of grain sintering could have reached an extreme. With further increasing the P/Ti ratio beyond 0.15, the mesoporous framework is still maintained, while more surface titanium phosphate phase might have occupied the internal pore space, slightly decreasing the surface area and pore volume.

The morphologies of titania and the in-situ P-TiO_2 catalysts were observed by TEM and SEM/SEM-EDX (Fig. 4). Pure titania consisted of relatively large grains (ca. 15 nm in size) with a smooth surface morphology. Its porosity is limited and from the interparticle voids due to the aggregation of titania grains (Fig. 4a). In comparison, P-TiO_2 samples (0.10 P-TiO_2 and 0.15 P-TiO_2) exhibit much higher porosity with rough morphology and channel-featured mesopores (ca. 3 nm; Fig. 4b-c and Table 1), in line with the results revealed by low-angle XRD (Fig. S1) and N_2 adsorption-desorption isotherms (Fig. S2 and Table 1). The SEM image of 0.15 P-TiO_2 further illustrates the morphology of the aggregated catalyst particles (Fig. 4d), and the EDX shows a uniform and rich distribution of P, Ti, O elements over the catalyst surface (Fig. 4e), supporting the presence of the surface titanium phosphate phase.

3.1.2. *Surface chemical state and acidic properties*

The high-resolution XPS spectra of Ti, P and O taken on the surface of titania, 0.05 P-TiO_2 and 0.15 P-TiO_2 are shown in Figs. 5 and S3. Ti $2p_{3/2}$ in TiO_2 is fitted as two peaks at 459.3 and 458.8 eV (Fig. 5a) with an atomic ratio of 0.028, indicative of two different chemical environments of surface Ti ions. Ti ions at 458.8 eV correspond to an octahedral coordination with oxygen, and those at 459.3 eV are in a tetrahedral environment [57,61,67–69]. For P-TiO_2 samples, the Ti $2p_{3/2}$ peak shifts from 458.9 eV for TiO_2 to 459.0 eV and is also broad (consisting of two fitted peaks). The peak denoting the tetrahedrally coordinated Ti ions increases in intensity with increased P loading, as the atomic ratio of surface Ti ions at 459.3 eV to that at 458.8 eV increases from 0.028 for TiO_2 to 0.254 for 0.05 P-TiO_2 and 0.351 for 0.15 P-TiO_2. Similar peak shifting and intensity variation were also observed for Ti $2p_{1/2}$ peak. In 0.50 P-TiO_2 as the reference sample, this atomic ratio is further increased to 1.14 (cf. Fig. S4), which also suggests the co-presence of both tetrahedral and octahedral Ti ions at such a high P loading. Although the possibility that a part of the octahedral Ti ions in P-TiO_2 is from titanium phosphate phase could not be excluded, the increase of this ratio at higher P loadings indicates that at least a large portion of Ti ions in titanium phosphate phase are present in a tetrahedral coordination. Moreover, with increased P loading, the ratio of tetrahedral to octahedral Ti ions increased as more titanium phosphate phase accumulated on the surface region. The O 1 s region of TiO_2 is composed of two peaks at 530.0 eV and 532.0 eV (Fig. 5b), corresponding to the Ti-O bond in TiO_2 and hydroxyl groups, respectively. The broad O 1 s spectra of P-TiO_2 can be fitted as four peaks, including Ti-O at 530.3 eV, P-O at 531.4 eV, O-H at 532.2 eV and C-O at 533.3 eV [57,58]. The C-O peak could be from carbon residues in the catalyst (e.g., the P123 template, ethanol or titanium butoxide). The slight shift of peaks of Ti-O and O-H to higher binding energy in P-TiO_2 is because of the partial transfer of electron cloud from O to P. The P $2p_{3/2}$ binding energy of P-TiO_2 was observed at 133.6 eV (Fig. S3), a characteristic peak from phosphate with phosphorus existing in a pentavalent-oxidation state [70]. The presence of Ti-P bond was excluded as the characteristic binding energy of P in TiP (titanium phosphide) at 128.6 eV was not observed [71].

In principle, phosphate species introduced into titania endows higher acidity. Phosphate species with high electronegativity attracts electron

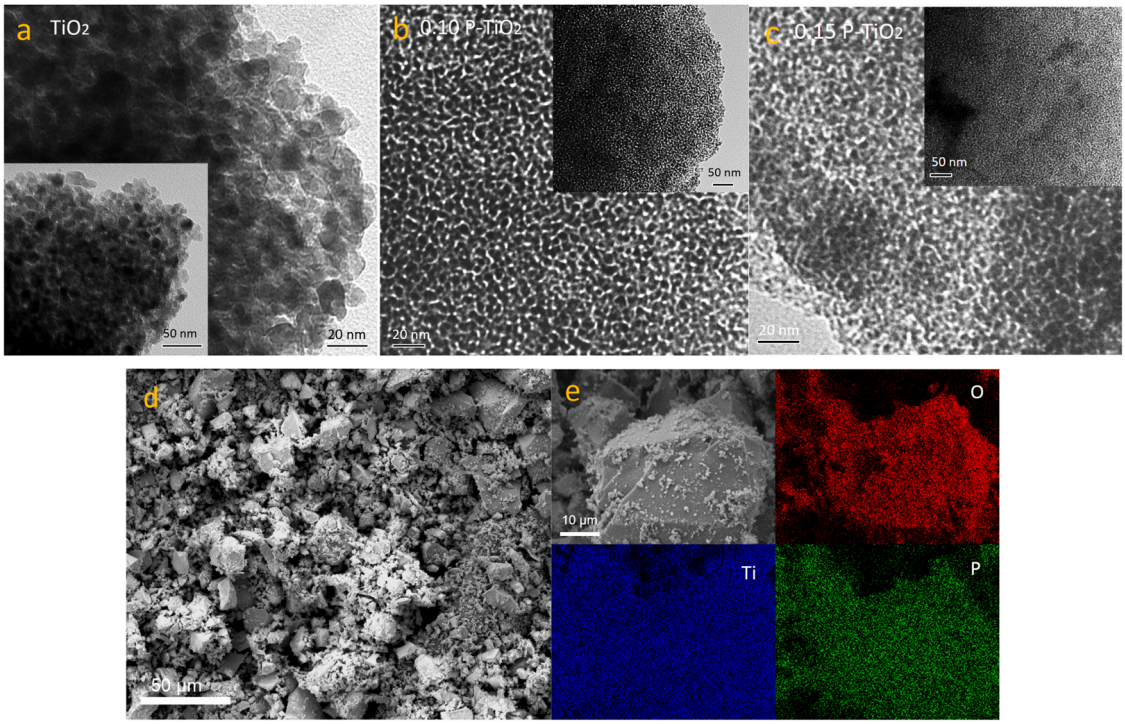

Fig. 4. Morphology of titania and P-TiO_2 catalysts. (a-c) TEM images of TiO_2, 0.10 P-TiO_2 and 0.15 P-TiO_2; (d and e) SEM images of 0.15 P-TiO_2 and the corresponding EDX elemental mapping.

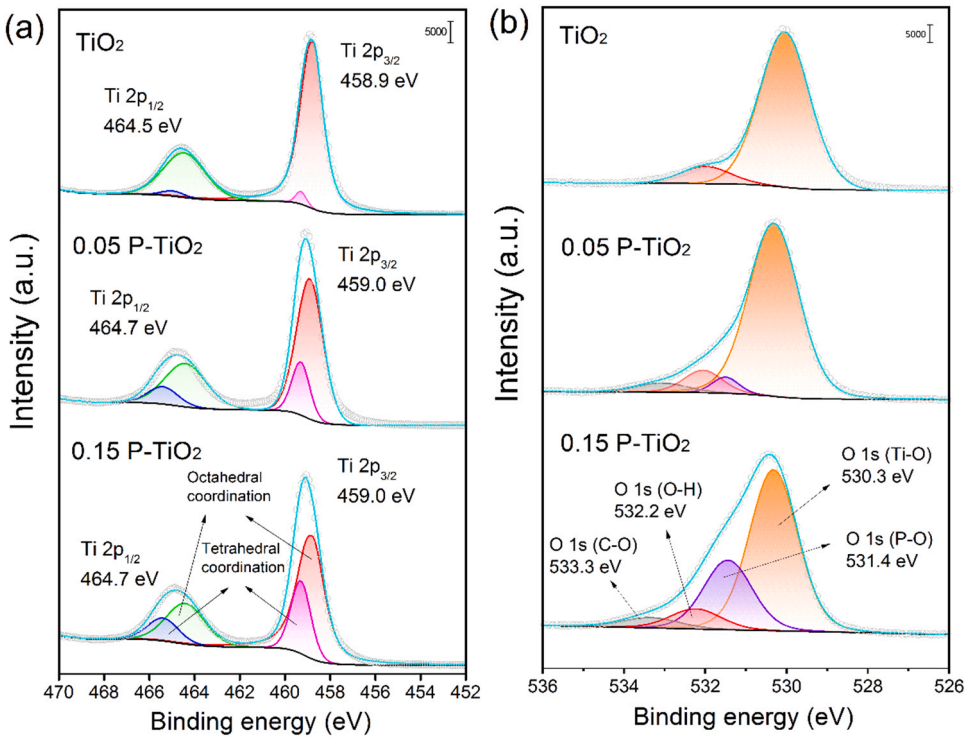

Fig. 5. High-resolution XPS spectra of (a) Ti 2p and (b) O 1 s regions taken on the surface of TiO_2, 0.05 P-TiO_2 and 0.15 P-TiO_2.

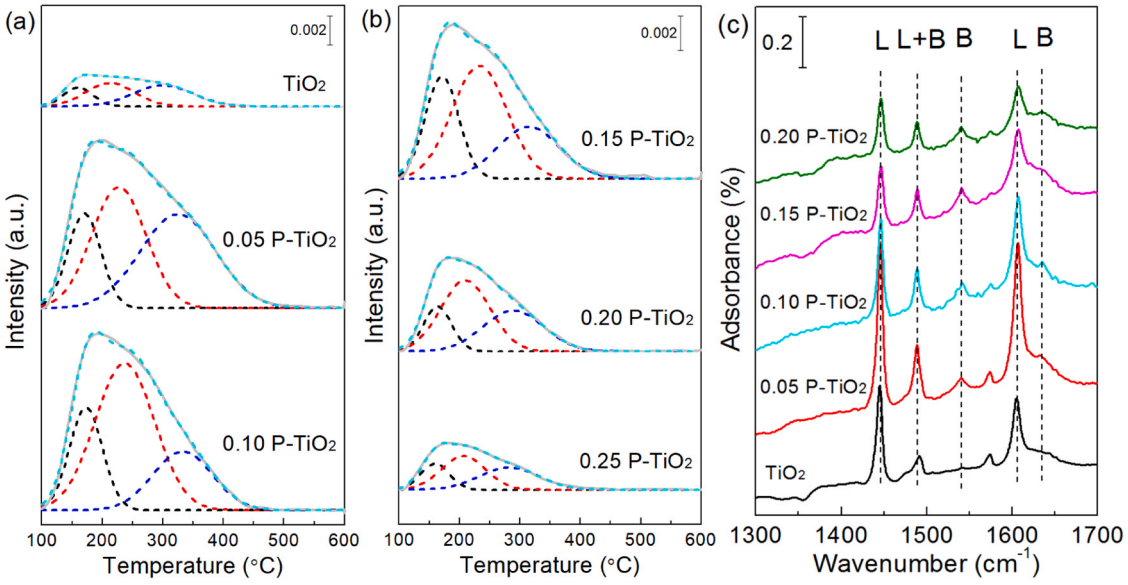

Fig. 6. Acidity characterization of the in-situ P-TiO_2 catalysts with different P loadings. (a and b) NH_3-TPD curves of the catalyst. Gray solid lines denote the experimental data; cyan dash lines denote the fitted cumulative curves; black, red and blue dash lines represent the deconvoluted profiles. (c) FTIR spectra of the adsorbed pyridine on the catalyst (pyridine evacuated at 150 °C). LAS is denoted by L and BAS by B.

cloud from the titania support, resulting in electron-deficient unsaturated Ti^{4+} centers behaving as LAS and hydroxyl groups attached to P that function as BAS. The total acid content and the distribution of acid strength of P-TiO_2 catalysts were investigated by NH_3-TPD (Fig. 6a–b and Table 2). All samples exhibit an overall broad NH_3 desorption peak before 400 °C, which is deconvoluted into three desorption peaks corresponding to acid sites of different strengths: two peaks at 100–250 °C were assigned to weak acid sites, one wide peak at 250–350 °C assigned to moderate acid sites, and no desorption peak of strong acid sites over 400 °C was found. The absence of strong acid sites corroborates water-tolerance of titania and P-TiO_2 catalysts, as strong LAS tends to form adducts with water molecule, resulting in a lower density of effective LAS in aqueous reaction media [24,32]. Generally, the total acidity of P-TiO_2 is much higher than that of pure titania (Table 2). However, it decreased with increasing the P loading, due to the lower surface area and porosity (Table 1) as well as the formation of more surface titanium phosphate phase causing less titania phase and Lewis acidic Ti^{4+} thereof exposed (vide infra).

The types and amounts of surface acid sites on P-TiO_2 catalysts were further determined from pyridine-IR spectra (Fig. 6c and Table 2). The

Table 2
Surface acidic properties and adsorption capacity of P-TiO_2 catalysts.

Entry	Sample	Acidity[a] (μmol NH_3/g)	Acidity (μmol pyridine/g)[b]			Adsorption (μmol/g)[c]		
			Brønsted	Lewis	B/L	Glucose	Fructose	HMF
1	TiO_2	110	0	89	0	41	99	184
2	0.05 P-TiO_2	488	30	165	0.18	44	85	66
3	0.10 P-TiO_2	472	37	79	0.46	32	131	40
4	0.15 P-TiO_2	387	51	73	0.70	30	128	39
5	0.20 P-TiO_2	232	50	65	0.77	31	140	39
6	0.25 P-TiO_2	121	n.d.[d]	n.d.[d]	n.d.[d]	29	139	39
7	0.05 P-TiO_2/Si	316	80	91	0.88	37	118	56
8	0.10 P-TiO_2/Na	23	0	107	0	51	147	54

[a] Determined by NH_3-TPD.
[b] Determined by pyridine-IR (at an evacuation temperature of 150 °C).
[c] 20 mg catalyst was added in 10 mL 0.01 M aqueous solution of glucose, fructose or HMF and stirred for 24 h at room temperature. Adsorption was calculated by the reduced amount of substrate in the solution.
[d] Not determined.

bands at 1540 and 1635 cm^{-1} are attributed to pyridine protonated on BAS, the bands at 1446 and 1606 cm^{-1} are assigned to pyridine adsorbed on LAS, and the absorbance at 1489 cm^{-1} is assigned to pyridine on both LAS and BAS [72]. The pure titania sample shows only LAS. With increased P loading, the Brønsted acid-related absorbance bands increase gradually until a P/Ti ratio of 0.15 and level off for higher P loadings. Simultaneously, a highest intensity of Lewis acid-related absorbance was observed for 0.05 P-TiO_2 (attributed to the co-existence of titania and titanium phosphate phases), followed by a sharp decrease for 0.10 P-TiO_2 and slightly decrease at higher P loadings (with reduced titania phase) (Table 2). The acid property of the in-situ P-TiO_2 here is significantly different from that reported for the post P-TiO_2. For example, the post-phosphation leads to a promoted Brønsted acidity, but accompanied by the drastic decrease of Lewis acidity [35], possibly due to the surface phosphate species covering LAS on titania. No impact of post-phosphation has been also reported on the acid properties [34], possibly because Ti-O-$PO(OH)_2$ formed by esterification between H_3PO_4 and –OH group on the anatase surface possessed only weak protons that neither acted as BAS, nor covered LAS due to its limited amount. Furthermore, the strength of LAS and BAS was also studied by recording the IR spectra of pyridine adsorbed on the samples under different evacuation temperatures, as shown in Fig. S5a for 0.10 P-TiO_2 as a representative sample (spectra for other samples give similar trend and are not shown for brevity). It is found that pyridine desorbed significantly at higher evacuation temperatures, e.g., the Lewis acidity was reduced by 70% and all Brønsted acidity disappeared at 350 °C (compared to that at 150 °C). This implies that the majority of LAS and all BAS are of mild acid strength, in line with the NH_3-TPD results (Fig. 6a–b).

It should be noted that the results from NH_3-TPD and pyridine-IR are to some extent different in the total acidity, particularly at higher P loadings. For example, for P/Ti ratios of 0.05, 0.10, 0.15 and 0.20, their total acidity measured by pyridine-IR is respectively 195, 116, 124 and 115 μmol pyridine/g, whereas that measured by NH_3-TPD is respectively 488, 472, 387 and 232 μmol NH_3/g (Table 2, entries 2–5). This difference might be due to a much higher response sensitivity of NH_3-TPD towards LAS in titanium phosphate phase than pyridine-IR, as the smaller NH_3 molecule could be easier to diffuse, adsorb and be confined in the interlayers of titanium phosphate phase, and be more difficult to desorb from the catalyst, causing a certain deviation from the actual case in the NH_3-TPD results. Comparatively, the pyridine-IR results are more reasonable revealing only a slightly decreased acidity at P/Ti ratios above 0.15, as supported by the somewhat similar performance in glucose conversion among 0.15, 0.20 and 0.25 P-TiO_2 catalysts (cf. Section 3.2). The further increase of surface P/Ti atomic ratio (measured by XPS which is with a certain detection depth of several nm) in the catalyst with P/Ti ratios above 0.15 is possibly attributed to the layer-wise accumulation of titanium phosphate phase on the surface, whereas a full coverage of titanium phosphate could have already reached and the exposed acid sites therein did not vary a lot. The slightly decreased total acidity therein according to pyridine-IR (Table 2) is due to the lower BET surface area and porosity at P/Ti ratios over 0.15.

As a result of acidity change with P loading, the adsorption capacity of glucose, fructose and HMF on the catalyst varies (Table 2). Generally, HMF has the highest adsorption on isolated LAS of TiO_2, whereas fructose is the most adsorbed on P-TiO_2. With increased P loading, HMF adsorption tended to monotonously decrease, and glucose adsorption has a similar evolution trend with the Lewis acidity (i.e., increased until a P/Ti ratio of 0.05 and afterwards slightly decreased), which is opposite to that of fructose adsorption. It is known that glucose is much more stable and less reactive than fructose on both LAS and BAS [9], and this is also reflected in its smaller adsorption than fructose on titania or P-TiO_2 catalysts (Table 2). In addition, BAS on P-TiO_2 is of weak strength and limited amount (Fig. 6 and Table 2), which catalyzes fructose but has little activity for glucose conversion (vide infra). This also explains the general increase of fructose adsorption on P-TiO_2 catalysts with higher P loadings (i.e., higher amounts of BAS). With increased P loading, generally the adsorption of glucose, which is reactive only on LAS, also decreases. This is attributed to the lower amount of LAS at higher P loadings (Table 2).

Based on XRD, FTIR and XPS results (Figs. 2, 3 and 5), structural insights were obtained into the anatase titania and in-situ P-TiO_2, as depicted in Scheme 2. The surface of anatase titania consists of saturated TiO_6 octahedra, and TiO_4 tetrahedra with unsaturated coordination spheres acting as LAS (Scheme 2a). The surface of P-TiO_2 catalyst consists of titania phase and the amorphous titanium phosphate phase, the relative amount of which depends on the P loading. The titanium phosphate phase contains TiO_4 tetrahedra as LAS and protonated PO_4 tetrahedra as BAS, both of which are closely arranged in a molecular-level proximity (Scheme 1, structure IV) forming Lewis-Brønsted acid pairs. Therefore, LAS on P-TiO_2 can be divided into two groups: isolated LAS on the titania phase and paired LAS (with the adjacent BAS) on the titanium phosphate phase (Scheme 2b). The increase of P loading leads to a gradual increase of surface titanium phosphate phase and thus the increased amount of Lewis-Brønsted acid pairs, simultaneously reducing the amount of titania phase and isolated LAS. This explains the evolution of acidity with the P loading, e.g., the BAS/LAS ratio in P-TiO_2 increases with the increasing P/Ti ratio and seems to level off at 0.7–0.8 for ratios above 0.15 (Table 2), where the surface of P-TiO_2 possibly reached a full coverage of titanium phosphate phase.

3.2. Glucose conversion to HMF in the batch reactor

The typical glucose conversion network via tandem catalysis over Lewis and Brønsted acids in water is illustrated in Scheme 3. Generally, glucose is epimerized to mannose and isomerized to fructose under

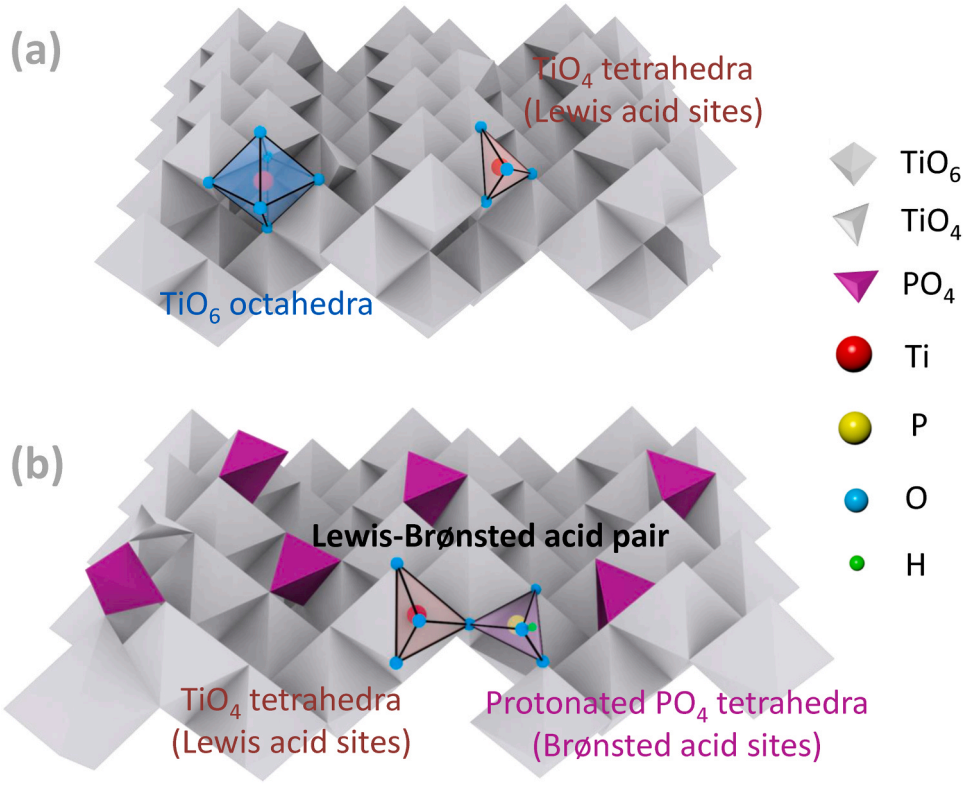

Scheme 2. Schematic representation of the surface structure of (a) anatase TiO_2 and (b) the in-situ phosphated titania catalyst.

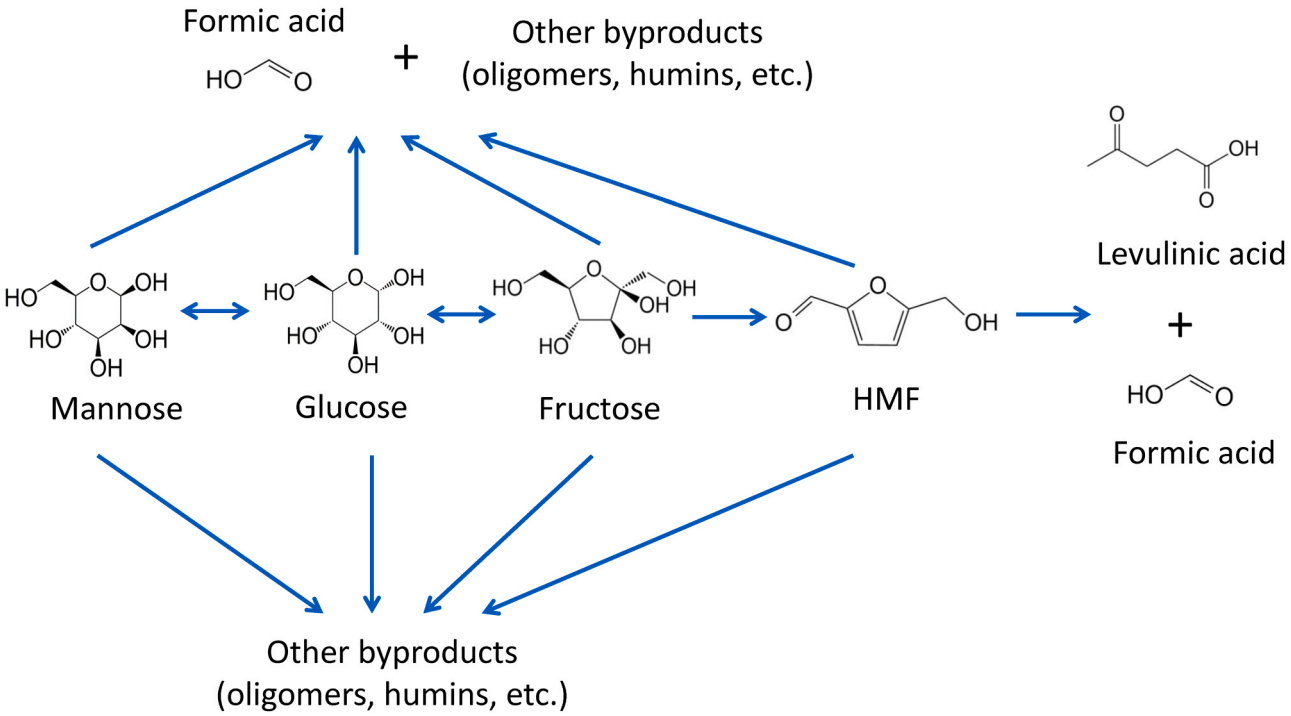

Scheme 3. Reaction network of glucose conversion in water over Lewis and Brønsted acid catalysts.

catalysis of Lewis acids, followed by fructose dehydration to HMF and HMF rehydration to formic acid (FA) and levulinic acid (LA) over Brønsted acids. Simultaneously, all sugars and HMF can be degraded to FA and polymerized to soluble oligomers or insoluble humins [12,73]. Other reaction routes such as the direct glucose dehydration without isomerization step [33,39] are excluded here as fructose has been clearly observed throughout all experiments (vide infra).

Fig. 7 shows the obtained results of glucose conversion in a water (with 20 wt% NaCl)-mTHF biphasic system over P-TiO_2 catalysts with different P loadings in the batch reactor at an optimized temperature of 150 °C (cf. more details in Fig. S7 regarding the temperature optimization). Fructose and mannose (the isomerization and epimerization

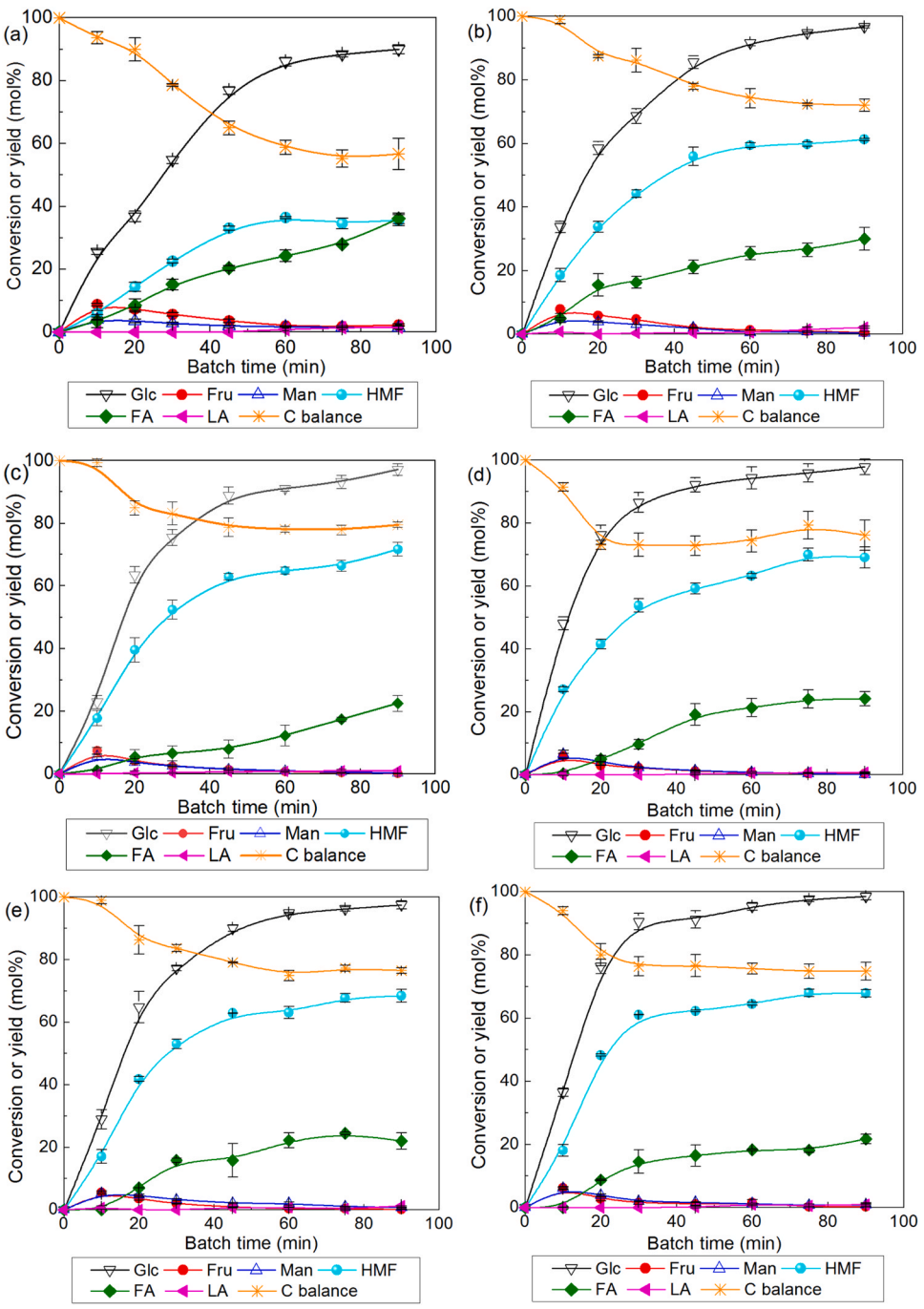

Fig. 7. Glucose conversion to HMF in the batch reactor over the prepared catalysts with different P loadings: (a) pure titania; (b) 0.05 P-TiO_2; (c) 0.10 P-TiO_2; (d) 0.15 P-TiO_2; (e) 0.20 P-TiO_2 and (f) 0.25 P-TiO_2. Reaction conditions: 150 °C, 0.1 M Glc, 20 wt% NaCl, 1 mL water and 4 mL mTHF, weight ratio of catalyst to glucose at 1:1. In the legend, Glc, Fru, Man, FA and LA represent glucose, fructose, mannose, formic acid and levulinic acid, respectively (the same for Table 3 and Fig. 11 hereafter). Error bars represent the standard deviation based on experiments in at least duplicate.

products from glucose, respectively) were formed over LAS at the early stage of the reaction, followed by their gradual dehydration to HMF or conversion to other byproducts such as FA and humins. The HMF yield increased steadily with the reaction progress and seemed to level off at the late stage of the reaction at high glucose conversions over 90%. HMF was stabilized by the biphasic system, where the mTHF phase extracted the majority of HMF further assisted by the salt addition via the salting-out effect (e.g., the partition coefficient of HMF at 150 °C was measured to increase from 1.01 to 2.17 after adding 20 wt% NaCl; cf. Section S2.2 of the Supplementary Material) and prevented it from side reactions in water such as its rehydration to FA and LA and degradation to FA and humins (Scheme 3). This led to a significant increase of the (maximum) HMF yield compared with the monophasic water system (see Fig. S8 and further discussions thereof in the Supplementary Material). Only a small amount of LA (< 2%) was observed during the reaction in the biphasic system, indicating little contribution of the typical Brønsted acid-catalyzed HMF rehydration. Comparatively, a large amount of FA (with respect to LA) was observed during the reaction especially at the late stage, accompanied by the humin formation as inferred from the carbon loss. The carbon balance (Eq. 6) first decreased gradually and then kept stable at the late stage of the reaction, in line with the nearly stable HMF yield thereof.

Under catalysis of titania which possesses only Lewis acidity, the maximum HMF yield is around 36% with the glucose conversion over 90% (Fig. 7a). This indicates that isolated LAS on titania also catalyzed fructose dehydration to HMF, but with a low selectivity. The carbon balance which stayed below 60% at the end of the reaction suggested a large amount of humin formation. Comparatively, all P-TiO_2 catalysts

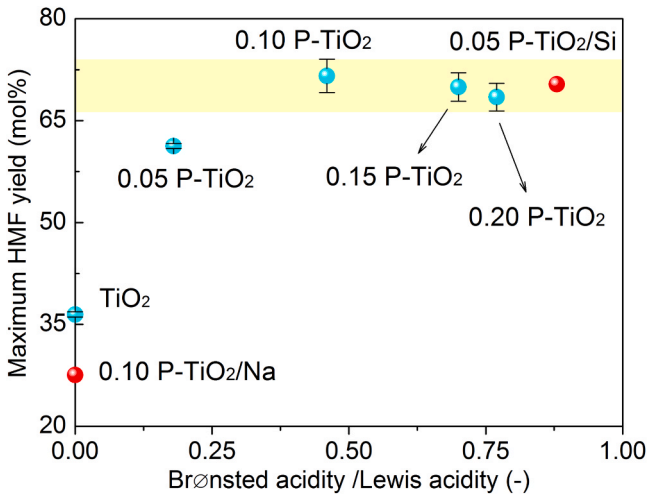

Fig. 8. Maximum HMF yield as a function of the ratio of Brønsted to Lewis acidity of the in-situ P-TiO_2 catalysts (determined by pyridine-IR as shown in Table 2).

exhibit a higher activity for glucose conversion (Fig. 7b-f). Particularly, with the increase of P loading, the maximum HMF yield increased and reached over 70% for P/Ti ratios above 0.10. Simultaneously, the maximum FA yield decreased from near 40% over titania to ca. 20% over 0.10 P-TiO_2, and levelled off for higher P loadings. The lower maximum HMF yield but higher FA yield at lower P loadings (TiO_2 and 0.05 P-TiO_2) is attributed to the promoted degradation and polymerization of sugars/HMF to FA and humins by the extra isolated unselective LAS (Table 2) [40]. The maximum HMF yield as a function of BAS/LAS ratio for P-TiO_2 catalyst is further summarized in Fig. 8. With increased BAS/LAS ratio, the maximum HMF yield increased gradually to 73% at an optimum acid ratio of ca. 0.5 (over 0.10 P-TiO_2), and then decreased slightly at higher acid ratios possibly related to the decreased total acidity over 0.15 and 0.20 P-TiO_2 catalysts (Table 2).

3.3. *Insights into bi-functionality of the in-situ phosphated titania catalyst*

Besides the relative abundance of LAS and BAS as discussed in Section 3.2 and most literature, this section further addresses the effect of proximity between LAS and BAS on their cooperativity, as well as insights into the role of individual LAS or BAS on the in-situ P-TiO_2 in glucose conversion network.

3.3.1. *Proximity between Lewis and Brønsted acid sites*

The proximity effect between LAS and BAS was studied by performance comparison between physical combinations of Lewis and Brønsted acid catalysts (i.e., TiO_2 +H_3PO_4 or TiO_2 +Amberlyst 16) and 0.10 P-TiO_2 in the biphasic system at 120 °C (to avoid the thermal decomposition of Amberlyst-16 occurring at 130 °C). For each catalyst combination, the amounts of LAS and BAS were calculated and maintained the same as those of 0.10 P-TiO_2 based on the pyridine-IR results (Table 2). As such, the main difference among these combinations is the proximity between LAS and BAS. TiO_2 was used as a benchmark to represent the mono-functional solid Lewis acid catalyst, the loading of which was adjusted to provide the same amount of LAS as in the other catalyst combination. The results and detailed discussion are provided in Fig. S9 and Section S2.4 of the Supplementary Material. Generally, the cooperative effect of LAS and BAS depends strongly on their proximity. Separated BAS (e.g., in TiO_2 +Amberlyst 16) improved the HMF yield, but had little effect on the overall activity for glucose conversion. BAS closely adjacent to LAS (e.g., at a molecular proximity in 0.10 P-TiO_2) promoted both the activity and HMF selectivity, due to the fast transfer of fructose to BAS for its dehydration to HMF, which decreased the occupancy of fructose on LAS leading to humins and increased accessibility of LAS for another glucose turnover.

3.3.2. *Roles of LAS and BAS: study on the effect of silylation and sodium ion exchange*

At low P loadings (e.g., 0.05 P-TiO_2), the surface acid sites consist of both isolated LAS and closely arranged Lewis-Brønsted acid pairs (Section 3.1). Consistently, the lower HMF yield over 0.05 P-TiO_2 (Fig. 8) results from unselective condensation of sugars/HMF into humins over the isolated LAS. Therefore, eliminating the excess isolated LAS is expected to give a lower glucose conversion rate but a higher HMF selectivity. To confirm this, silylated 0.05 P-TiO_2 (0.05 P-TiO_2/Si; cf. Section 2.3) was tested as the catalyst for glucose conversion, which possesses a higher Brønsted acidity but fewer Lewis acidity than 0.05 P-TiO_2, as revealed by pyridine-IR and NH_3-TPD (cf. entries 2 and 7 of Table 2, Figs. S5b and S6a). Fig. 9 exhibits the performance comparison between these two catalysts, and the TOF values of sugars and HMF (Eq. 3) are summarized in Table 3. The removal of isolated LAS in 0.05 P-TiO_2/Si led to higher TOF values of glucose and HMF. As a result, the HMF selectivity was significantly improved with the maximum HMF yield being increased from 61% in 0.05 P-TiO_2 to 70% in 0.05 P-TiO_2/Si (Fig. 9), which is close to that with higher P loadings (Fig. 8).

Furthermore, BAS on the in-situ P-TiO_2 catalyst was eliminated by exchanging with sodium ions (0.10 P-TiO_2/Na; cf. Section 2.3). Na-exchange led to not only the disappearance of BAS, but also an increased amount of LAS with decreased acid strength (cf. entries 3 and 8 of Table 2), as revealed by its pyridine-IR results showing a significant desorption of the adsorbed pyridine at higher evacuation temperatures (e.g., the Lewis acidity is reduced by over 80% at 250 °C; Fig. S5c), and is consistent with the NH_3-TPD pattern indicating only a weak desorption peak at 100–150 °C for 0.10 P-TiO_2/Na (Fig. S6b). This finding can be explained by a change in the electronic state of Ti^{4+} after exchange of an adjacent proton with Na^+. Concretely, protons compete with the Ti^{4+} LAS for electrons of oxygen, therefore, Na-exchange should lead to the decrease in the positive charge over Ti and thus the lower strength of LAS [40].

Performance comparison between 0.10 P-TiO_2 and 0.10 P-TiO_2/Na for the conversion of glucose or fructose is given in Fig. S10 and discussed in detail in Section S2.5 of the Supplementary Material. Generally, for glucose conversion, a lower activity of 0.10 P-TiO_2 than 0.10 P-TiO_2/Na was observed, which is attributed to the relatively stronger LAS on 0.10 P-TiO_2 being less active in water. Despite the higher glucose conversion and fructose yield over 0.10 P-TiO_2/Na (Figs. S10 a and b), the HMF yield is far lower over the isolated unselective LAS of this catalyst than that over Lewis-Brønsted acid pairs on the 0.10 P-TiO_2 catalyst (Fig. S10c).

For fructose conversion, 0.10 P-TiO_2 gave higher activity and HMF yield than 0.10 P-TiO_2/Na (Figs. S10 a and c), due to the promoted fructose dehydration to HMF by BAS over 0.10 P-TiO_2. Moreover, despite the faster conversion of fructose than glucose, fructose gave a far lower HMF yield than glucose over both 0.10 P-TiO_2 and 0.10 P-TiO_2/Na. This is attributed to the more active fructose adsorbing on LAS (Table 2) leading to humins, besides fructose dehydration to HMF over the adjacent BAS (on 0.10 P-TiO_2). Comparatively, glucose is more stable towards polymerization into humins over LAS, and is not converted over BAS (of weak acid strength).

3.4. *Relationship between the synthesis method, structure, acidic property and reaction performance of the in-situ phosphated titania*

By employing sol-gel synthesis featuring the in-situ phosphation in this work, titanium butoxide hydrolyzed fast to titanium hydroxide (which was further condensed to form titania particles) in the presence of phosphoric acid in aqueous ethanol solution. This process was accompanied by the condensation reaction between phosphoric acid and the surface Ti-OH of the as-prepared TiO_2. As a result, the phosphate

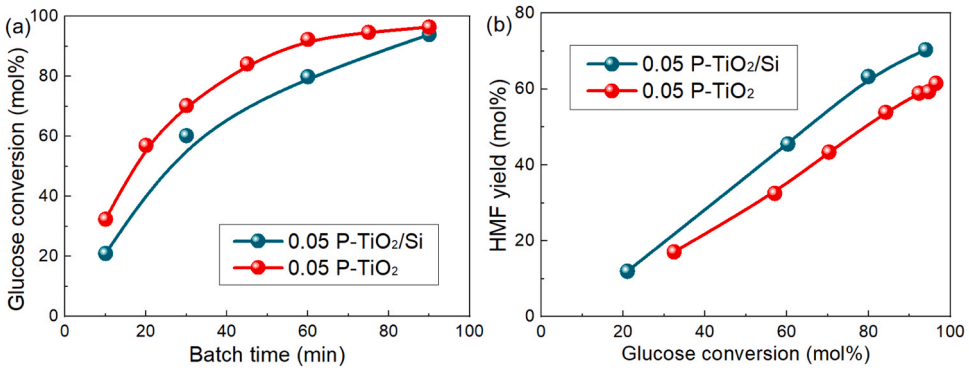

Fig. 9. Performance comparison between 0.05 P-TiO_2 and 0.05 P-TiO_2/Si for (a) glucose conversion and (b) HMF yield in the batch reactor. Reaction conditions: 150 °C, 0.1 M glucose, 20 wt% NaCl, 1 mL water and 4 mL mTHF, weight ratio of catalyst to glucose at 1:1.

Table 3
Performance comparison between titania, the in-situ P-TiO_2 and modified P-TiO_2 catalysts in the batch reactor[a].

Catalyst	X_{Glc} (mol%)	Y_{Fru} (mol%)	Y_{HMF} (mol%)	Initial reaction rates (μmol·min^{-1})			TOF[b] (min^{-1})		
				Glc	Fru	HMF	Glc	Fru	HMF
TiO_2	15.2	9.0	6.6	1.28	0.76	0.56	0.77	–	–
0.05 P-TiO_2	32.4	7.6	12.1	2.58	0.60	0.96	0.89	0.21	0.40
0.05 P-TiO_2/Si	21.0	6.4	12.0	1.86	0.57	1.06	1.14	0.35	0.58
0.10 P-TiO_2	22.9	8.0	17.8	1.89	0.66	1.47	1.33	0.46	0.70
0.10 P-TiO_2/Na	56.8	9.8	3.1	4.46	0.77	0.24	2.31	–	–

[a] Reaction conditions: 150 °C, 10 min, 20 wt% NaCl, 1 mL 0.1 M glucose (in water), 4 mL mTHF, weight ratio of catalyst to glucose at 1:1.
[b] Based on the amount of LAS (for glucose) or BAS (for fructose and HMF) measured by pyridine-IR (Eq. 3).

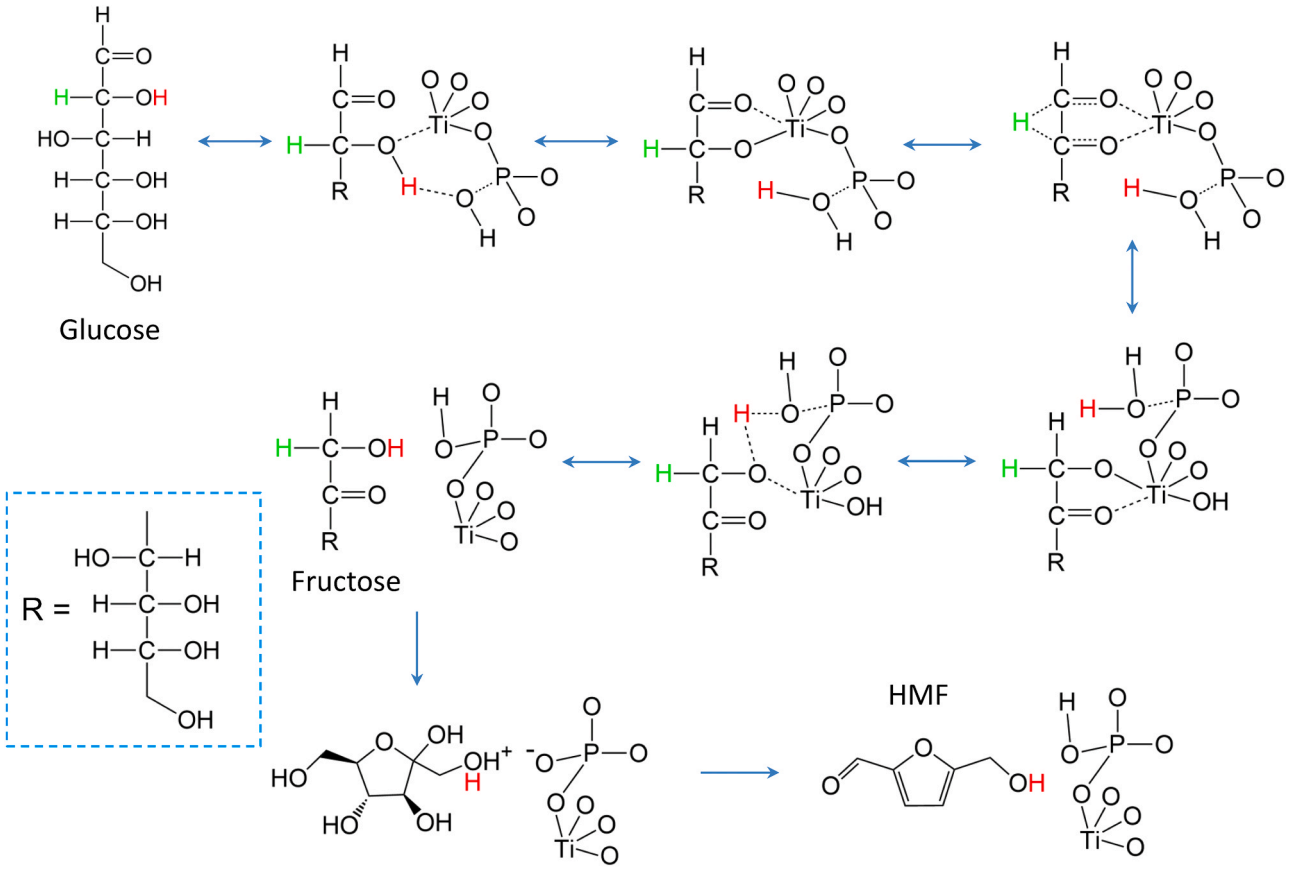

Scheme 4. Proposed mechanism of glucose conversion to HMF over Lewis-Brønsted acid pairs on the in-situ P-TiO_2 catalyst.

species was incorporated into the titania framework forming amorphous titanium phosphate phase as a surface layer embedded with anatase or amorphous titania phase (Scheme 2), as supported by XRD and FTIR results (Figs. 2–3). It is known that during the calcination, the rapid condensation between large amounts of surface Ti-OH on the as-prepared amorphous TiO_2 caused the collapse of its mesostructure [57]. In this work, the stabilization of the mesoporous framework by the direct phosphate incorporation can be attributed to (*i*) the more complete condensation of surface Ti-OH by H_3PO_4 and (*ii*) inhibition of TiO_2 crystallite grain growth by the interspersed surface amorphous titanium phosphate acting as a diffusion barrier.

XPS characterization (Fig. 5) shows that the surface of P-TiO_2 catalyst is composed of coordinately saturated octahedral TiO_6 units and unsaturated tetrahedral TiO_4 units (Scheme 2). The absence of open coordination sites in octahedral TiO_6 prevents Ti^{4+} to interact with reactant molecules, making it inactive. Comparatively, Ti^{4+} in TiO_4 unit has four (tetrahedral) or fewer bonds with oxygen (present in the support) to allow coordination with electron-donating groups of the substrate, e.g., carbonyls from glucose or fructose, thus acting as the catalytically active LAS [32]. The tetrahedral TiO_4 is from either titania phase or titanium phosphate phase. The former acts as isolated LAS, while LAS in the latter is in a close arrangement with the adjacent protonated phosphate group as mild BAS. The percentage of isolated LAS or Lewis-Brønsted acid pairs is tunable by adjusting the P loading. With increased P loading, the surface region tends to be composed of more amorphous titanium phosphate phase and thus isolated LAS from the titania phase is significantly reduced. Besides, all (Lewis) acid sites on P-TiO_2 catalysts are of weak or moderate strength ensuring their water-tolerance.

LAS is highly active for glucose conversion. However, isolated LAS in the titania phase is unselective towards HMF. Particularly, fructose has the largest adsorption on titania and P-TiO_2 catalysts, and is highly inclined to form humins over LAS. In the titanium phosphate phase, the protonated phosphate group (BAS) adjacent to the TiO_4 tetrahedra (LAS) on a molecular level significantly improved the glucose conversion and HMF yield, by timely dehydrating the desorbed fructose and suppressing its re-adsorption on LAS (leading to humins), faster liberating LAS for another glucose turnover. Based on the reported mechanism of glucose isomerization over Lewis acid in water [12,74], a mechanism of glucose conversion over Lewis-Brønsted acid pairs on the present P-TiO_2 catalyst is proposed in Scheme 4. Glucose is isomerized to fructose over LAS via an intramolecular hydride shift, where the adjacent protonated phosphate group participates by transfer of a hydride between the oxygen of the first and second carbon. The formed fructose is then desorbed and fast dehydrated by the proton from the adjacent phosphate group.

Notably, although a desirable HMF yield over 70% was obtained by the bi-functional P-TiO_2 catalyst, still ca. 30% of the overall carbon was lost to among others humins (Fig. 7). Considering the adsorption and reactivity of fructose as well as HMF on the catalyst, it is believed that still a part of fructose molecules were converted to humins even over Lewis-Brønsted acid pairs. Besides, the overall Brønsted acidity is lower than Lewis acidity for all P-TiO_2 samples (since the BAS/LAS ratio is lower than 1; Table 2), indicating still the presence of isolated LAS on these catalysts. Moreover, beyond the optimal BAS/LAS ratio (over 0.10 P-TiO_2), the excess BAS might also promote the humin formation.

3.5. Glucose conversion to HMF in the packed-bed microreactor

0.10 P-TiO_2 catalyst, which gave the best performance in the batch reactor, was further loaded into the microreactor for the continuous synthesis of HMF from glucose. The glucose conversion and HMF yield as a function of the inverse weight hourly space velocity (1/*WHSV*; Eq. 5) under different catalyst loadings and glucose concentrations are shown in Fig. 10 (cf. Fig. S11 for the corresponding FA and LA yields). For a given catalyst loading, the glucose conversion increased with 1/*WHSV* and approached 100% at sufficiently small values of *WHSV* (Fig. 10a), due to the prolonged contact time with the catalyst. A maximum HMF yield of 72% from 0.1 M glucose feedstock was found with a moderate catalyst loading of 1.3 g. However, with increased 1/*WHSV*, the HMF yield dropped at the late stage of the reaction, in contrast to batch reactions where the HMF yield kept stable with prolonging time at high glucose conversions (Fig. 7). In the batch reactor, the catalyst powders were uniformly dispersed only in the aqueous phase due to the hydrophilic nature of titania-based catalysts (Fig. S12a). The formed HMF then desorbed from the acid sites, diffused to the aqueous phase, and was subsequently extracted to the mTHF phase. As the organic phase did not contact the catalyst, the extracted HMF was prevented from side reactions. In the microreactor, a slug flow containing the aqueous droplets and continuous organic slugs was observed at both the inlet and outlet of the packed bed (Figs. S10 b-c). Thus, both phases might contact the catalyst when flowing through the bed (see more explanations below). As a result, HMF in mTHF might be further converted into byproducts (e.g., humins), lowering the HMF yield at the late stage of the reaction. This hypothesis was corroborated by the results of control experiments in batch using 0.1 M HMF as the substrate, where the HMF conversion at 150 °C for 60 min was ca. 20% in the monophasic mTHF, but below 5% in the biphasic water-MTHF system (Table S2).

Under different catalyst loadings (0.6 – 2.6 g; particle size of ca. 0.3 – 0.425 mm), the *WHSV* value was kept equal by varying the two-phase mixture flow rate proportionally. At the same *WHSV*, the glucose conversion increased with increased catalyst loading (Fig. 10a) and the corresponding maximum HMF yield was reached faster (Fig. 10b). The performance difference here indicates mass transfer limitation at lower flow rates [75]. In addition, the glucose conversion and (maximum) HMF yield are also lower when using a higher glucose concentration

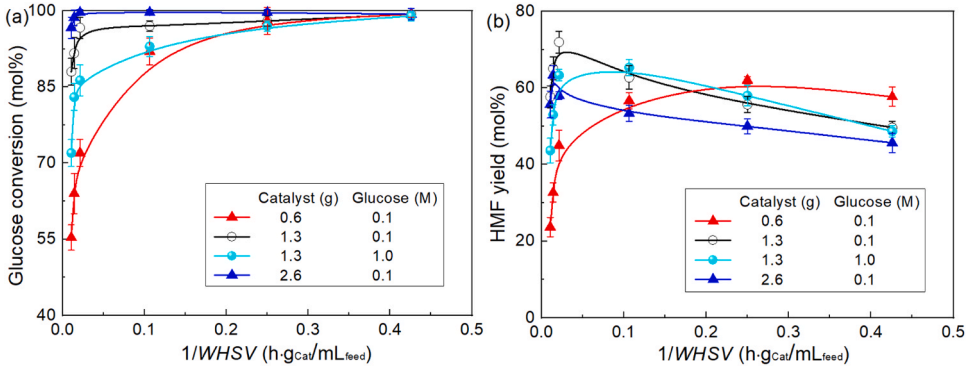

Fig. 10. (a) Glucose conversion and (b) HMF yield as a function of the inverse weight hourly space velocity (1/*WHSV*) at different loadings of 0.10 P-TiO_2 and glucose concentrations in the water-mTHF biphasic system in the packed-bed microreactor. Reaction conditions: 150 °C, 1 h time-on-stream, Q_{org}/Q_{aq} of 4. Error bars represent the standard deviation based on experiments in at least duplicate.

(1 M) for the same catalyst loading (1.3 g), which supports the presence of mass transfer limitation in the catalyst bed if one assumes that acid-catalyzed glucose conversion is first-order in reactant [8]. However, such mass transfer limitation should not be severe, as a close to full glucose conversion could still be quickly achieved under the lowest catalyst loading (0.6 g) by further raising the 1/*WHSV* value above 0.25 $h \cdot g_{Cat}/mL_{feed}$ (Fig. 10a), and the maximum HMF yield in this case is still high (ca. 66%; Fig. 10b).

The mass transfer of glucose (from water to catalyst) and HMF (between catalyst, water and mTHF) is related to not only the mixture flow velocity, but also the flow pattern of aqueous and organic phases through the bed. Since a hydrophobic PFA capillary microreactor was used, the organic phase existed as the continuous phase containing discrete aqueous droplets before the mixture reached the bed (Fig. S12b). This could have caused a local contact between the catalyst and mTHF in the beginning section of the bed. In addition, the local flow imperfection possibly caused by the imperfect catalyst packing or particle size non-uniformity could also trigger this unfavorable contact. However, in the main part of the bed, an inversion of flow configuration is expected. That is, the continuous phase in the bed (if long enough) has been switched to the aqueous phase (due to the hydrophilic nature of the catalyst) with the organic phase as droplets through the particle interstitial voids, possibly except the near-wall region due to the influence of PFA wall material. Thus, a local organic-catalyst contact could have been present in various parts of the current packed-bed microreactor, which decreased the glucose transport rate from the aqueous phase to the catalyst (since glucose is hardly soluble in mTHF) and led to degradation of the extracted HMF to some extent. As a result, at the increased mixture flow rate over the bed with increasing the catalyst loading from 0.6 to 1.3 g (i.e., under equal 1/*WHSV*), the mass transfer was improved leading to a higher glucose conversion and the corresponding improved (maximum) yield of HMF, as correctly illustrated in Fig. 10. However, further increasing the catalyst loading from 1.3 to 2.6 g at the same 1/*WHSV* led to a slightly lower (maximum) HMF yield (Fig. 10b), possibly because the mass transfer of HMF (in mTHF) to the catalyst was also enhanced under such a higher flow rate, leading to a slightly more significant degradation of the (extracted) HMF. To fully understand these reaction results, an in-depth hydrodynamic characterization of the packed-bed microreactor is necessary (to be addressed in ongoing studies).

3.6. *Evaluation of the stability and recyclability of the in-situ phosphated titania catalyst in the packed-bed microreactor*

Besides the activity, the stability and reusability of the prepared P-TiO_2 catalyst is also important for a potential scaled-up HMF production. The activity loss, if present, could be due to (i) the leaching of acid sites of P-TiO_2; (ii) the exchange of protons on the catalyst with Na^+ (NaCl) in water; and (iii) the accumulation of humins on the active acid sites. The phosphate leaching was usually tested via a hot filtration method in batch reactors [25,76]. That is, after running the reaction for a certain time and filtering out the solid acid catalyst, the reaction was continued in the absence of solid catalyst. The observation of no or some further reaction was used to prove no or some leaching of the active sites [76]. However, as discussed above, glucose conversion to HMF over the current catalyst is catalyzed by the synergistic effect of LAS and BAS. The phosphate species, if leached into water, would serve as the sole BAS that has no distinct effect on promoting the glucose conversion. Therefore, no further reaction detected after catalyst filtration is not sound enough to exclude the possibility of phosphate leaching. Besides, the reusability of solid catalyst was usually tested by running several consecutive batch-wise reactions in the presence of limited amount of substrate using the same catalyst, which is time-consuming and difficult to capture other factors causing the catalyst deactivation such as the humin deposition. Moreover, the activity loss is usually mingled with varying conversions over time during the reaction in batch. Therefore, here the catalyst deactivation behavior was studied in the packed-bed microreactor. The time-on-stream reaction results at different glucose concentrations over 0.10 P-TiO_2 are displayed in Fig. 11. The glucose conversion and HMF yield both gradually decreased, e.g., after a 5-hour running, the activity loss is around 15% and 29% for 0.1 M and 1 M glucose feedstock, respectively. After a simple regeneration treatment by calcination in air (Section 2.2), the activity of the catalyst re-packed in the microreactor returned significantly, though being slightly lower than that of the fresh catalyst. Subsequently, the activity of the 1st-regenerated catalyst can be fully recovered in the following regeneration cycles (Fig. 11).

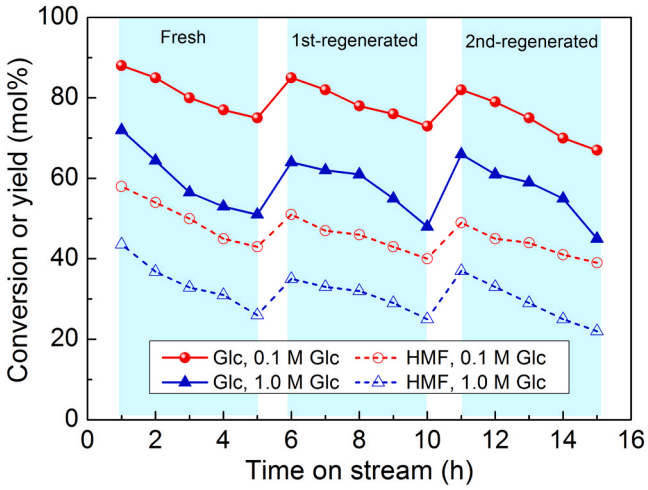

Fig. 11. Glucose conversion and HMF yield as a function of time-on-stream. Reaction conditions: 1.3 g 0.10 P-TiO_2, 150 °C, Q_{org}/Q_{aq} of 4. The two-phase mixture flow rate was constant at 2 mL/min with a (1/*WHSV*) of 0.011 $h \cdot g_{Cat}/mL_{feed}$.

The possibility of Na^+-exchange can be excluded as little amount of Na was found on the recycled catalyst (Table S3). This is attributed to the weak strength of BAS in the catalyst. Furthermore, ICP analysis of the aqueous phase after 1-hour reaction over the fresh catalyst indicates the presence of P (55 mg/kg), and P/Ti ratio of the catalyst decreased from 0.099 to 0.093 after 5-hour reaction, suggesting a small extent of phosphate leaching. However, after the first and second catalyst regeneration cycles and three 5-hour runs, little P (< 1 mg/kg) was detected in the aqueous phase and P/Ti ratio turned to be stable (Table S3). This implies that a tiny part of phosphates that were weakly anchored onto the surface in the fresh catalyst tended to hydrolyze and leached to water under hydrothermal reaction conditions at short time-on-stream, while the remaining phosphates were strongly incorporated into the framework and by far more stable towards hydrolytic leaching (in line with the literature results using titanium phosphate as the catalyst for glucose conversion [77,78]). The leaching of phosphates only led to a slight acidity loss (Table S3), explaining the slightly lower activity for the first-regenerated catalyst than that for the fresh one (Fig. 11). The color of catalyst bed was observed to change from white to dark brown after 5 h (Fig. S13), indicating the accumulation of humins on the catalyst that could cover the active acid sites and block inner pores. Particularly, at a higher glucose concentration, more humins were produced and thus led to a faster deactivation (Fig. 11). After a simple re-calcination to remove humins, the brown used catalyst returned to white (Fig. S13), accompanied by the recovered accessibility of acid sites and catalytic activity.

Table 4
Performance comparison of this work with P-TiO_2 catalysts in the literature[a].

No.	Phosphation method	Solvent system	Reactor type	Feedstock	T (°C)	t (min)	$WHSV_{Glc}$[b] (g_{Glc}/(g_{Cat}·h))	X_{Glc} (mol%)	Y_{HMF} (mol%)	STY_{HMF}[c] (mol min^{-1} m^{-3})	Source
1	Post	Monophasic aqueous THF[d]	Batch	0.05 M glucose	120	120	0.200	98	81.2	0.376	[34]
2	Post	Biphasic water-n-butanol	Batch	2 wt% glucose	175	180	1.111	97	81	0.500	[35]
3	Post	Biphasic water-THF[d]	Batch	5 wt% glucose	175	105	2.286	96.5	62.8	1.660	[36]
4	Post	Biphasic water-butanol	Batch	1 M glucose	120	240	0.800	29	18	0.208	[33]
5	Post	Biphasic water-MIBK	Batch	1 M glucose	120	240	0.800	41	14	0.162	[33]
6	Post	Biphasic water-SBP[e]	Batch	1 M glucose	120	240	0.800	49	34	0.393	[33]
7	In-situ[f]	Biphasic water-THF[d]	Batch	10 wt% glucose	175	120	2.000	98.5	53.5	0.495	[41]
8	In-situ[g]	Biphasic water-THF[d] + NMP[h]	Batch	5.5 wt% glucose	150	105	0.137	95.6	55.5	0.367	[42]
9	In-situ	Biphasic water-mTHF	Batch	0.1 M (2 wt%) glucose	150	90	0.667	97	73	0.162	This work
10	Post	Biphasic water-MIBK+NMP[h]	Packed bed	5 wt% cello-oligomer	220	40[i]	–	–	53	–	[36]
11	In-situ	Biphasic water-mTHF	Packed bed	0.1 M (2 wt%) glucose	150	60[j]	0.845	96	72	145.64	This work
12	In-situ	Biphasic water-mTHF	Packed bed	1 M (20 wt%) glucose	150	60[k]	1.694	93	66	291.96	This work

[a] In the table, T is the reaction temperature, and t the reaction time (in batch) or time on stream (in flow); X_{Glc} and Y_{HMF} represent the glucose conversion and HMF yield, respectively.
[b] $WHSV_{Glc}$ is the weight hourly space velocity regarding glucose, which was estimated for packed-bed (micro)reactors as the inlet mass flow rate of glucose divided by the packed catalyst weight, and for batch reactors as the initial mass of glucose divided by the product of the suspended catalyst weight and batch reaction time.
[c] The space time yield of HMF (STY_{HMF}) in the batch reactor is determined by $STY_{HMF} = N_{Glc,0} Y_{HMF}/(V_L t)$, where $N_{Glc,0}$ is the initial mole amount of glucose, V_L is the liquid volume in the reactor; STY_{HMF} in the packed-bed (micro)reactor is estimated by $STY_{HMF} = Q_{aq} C_{aq,Glc,0} Y_{HMF}/V_{Cat}$, where Q_{aq} and $C_{aq,Glc,0}$ represent the inlet flow rate of aqueous phase and glucose concentration, respectively, V_{Cat} is the volume of catalyst bed.
[d] Tetrahydrofuran.
[e] 2-Sec-butylphenol.
[f] P-TiO_2 was synthesized by hydrolyzing titanium iso-propoxide in the presence of H_3PO_4 in iso-propanol; a gel was formed after mixing titanium iso-propoxide, H_3PO_4 and water.
[g] P-TiO_2 was synthesized in flow by hydrolyzing titanium butoxide in the presence of H_3PO_4 in n-butanol; a slurry was obtained after mixing titanium butoxide, H_3PO_4 and NH_3/H_2O at 100 °C.
[h] N-methyl-2-pyrrolidone.
[i] At a liquid hourly space velocity (ratio of the liquid volumetric flow rate to the heated reactor volume) of 18.9 h^{-1}.
[j] WHSV = 46.9 mLfeed·gCat−1·h−1 (1.3 g 0.10 P-TiO2).
[k] $WHSV$ = 9.4 $mL_{feed}·g_{Cat}^{-1}·h^{-1}$ (1.3 g 0.10 P-TiO_2).

3.7. Performance comparison with the literature work and future perspective for microreactor optimization

The reaction performance of the prepared catalysts has been compared with the literature work that used post or in-situ P-TiO_2 catalysts for HMF synthesis from glucose in either batch or continuous flow reactors (Table 4) [33–36,41,42]. In this work, a maximum HMF yield of 73% was achieved from 0.1 M glucose in batch over 0.10 P-TiO_2 (after 90 min), and 66% was achieved from 1 M glucose in the continuous microreactor (1 h time-on-stream, $WHSV$ = 9.4 $mL_{feed}/(h·g_{Cat})$, 1.3 g 0.10 P-TiO_2), both at 150 °C. Several literature work reported a higher HMF yield over 80% in batch (entries 1 and 2), which however is believed to also benefit from the modified chemistry environment, since they either used THF as the reaction medium or n-butanol (having a high solubility in water being ca. 73 g/L at 25 °C) as the extraction solvent [34,35]. Compared with cases using water as the reaction medium in either batch or flow reactors (giving HMF yields of 18–62.8%), the current P-TiO_2 catalyst affords a (much) higher HMF yield (entries 3–12). Moreover, in this work HMF was synthesized and the catalyst deactivation behavior was studied more reliably in flow in a packed-bed microreactor, where the $WHSV$ value of glucose is relatively high and the space time yield of HMF is about two orders larger than that in batch reactors, indicating a significantly enhanced process efficiency (Table 4).

As previously discussed, the contact between the organic phase and catalyst bed caused the degradation of the extracted HMF. To reduce this unfavorable contact and further optimize the HMF yield, the upstream slug flow pattern might be finely tuned using a hydrophilic microreactor material (e.g., glass or stainless steel) rendering the aqueous phase as the continuous phase. Besides, the influence of catalyst packing and particle size distribution on the flow uniformity should be examined and optimized (still under our investigation). Furthermore, adjusting microreactor configuration and the form of catalyst incorporation to optimize the flow pattern represents another approach to improve the reaction performance. For example, the hydrophilic catalyst can be washcoated into the microreactor, so that the organic phase present as droplets would be surrounded by the aqueous solution as the continuous phase and thus is not in direct contact with the catalyst [46,48,79]. However, this strategy may require cumbersome coating techniques. Another method is to disperse nano- or micro-sized catalysts in the aqueous phase, together with the organic phase forming an aqueous slurry-organic slug flow pattern. Here, the possible cost is channel fouling or local blockage leading to device malfunction, and additional downstream catalyst recycling is needed [80]. For catalyst regeneration in among others the current packed-bed microreactor, a more convenient on-line approach can also be considered, e.g., via a mild oxidation of humins by H_2O_2 in flow [81].

4. Conclusion

This work presented an in-situ phosphation method for the synthesis of phosphated titania as the bi-functional solid acid catalyst for HMF synthesis from glucose. Phosphates were successfully incorporated into the titania framework, forming an amorphous titanium phosphate phase on the surface region embedded with anatase or amorphous titania phase. The coordinately unsaturated tetrahedral TiO_4 units on the titania phase and titanium phosphate phase act as water-tolerant LAS with mild acid strength. The titania phase possesses only the isolated LAS, while the titanium phosphate phase also contains the protonated phosphate groups as mild BAS that are closely arranged with LAS in a molecular-level proximity forming Lewis-Brønsted acid pairs. The isolated LAS is unselective towards HMF due to the dominant condensation reactions from sugars/HMF to humins in the absence of BAS. The cooperative effect of LAS and BAS depends on not only the relative abundance, but also their proximity. Lewis-Brønsted acid pairs on the in-situ phosphated titania catalyst render a higher activity for glucose conversion and HMF selectivity compared with other physically combined Lewis and Brønsted acid catalysts, attributed to a more selective tandem catalysis (i.e., fructose formed from glucose and desorbed from LAS was timely dehydrated to HMF over the adjacent BAS, reducing its re-adsorption on LAS leading to humins and facilitating the liberation of LAS for another glucose turnover). The increase of P loading could lead to more surface titanium phosphate phases and thus the increased amount of Lewis-Brønsted acid pairs, simultaneously reducing the isolated LAS from the titania phase. Under an optimized Brønsted to Lewis acidity ratio of ca. 0.5 (over 0.10 P-TiO_2), an HMF yield of 73% was achieved from 0.1 M glucose at 150 °C after 90 min in a water (20 wt% NaCl)-mTHF biphasic system in batch.

Flow reaction mode and catalyst deactivation were studied in a microreactor packed with the 0.10 P-TiO_2 catalyst. At 150 °C, the maximum HMF yield (72%) is comparable to that in batch from 0.1 M glucose with a moderate catalyst loading (1.3 g). However, mass transfer limitation is likely present to some extent, given the performance difference at the same $1/WHSV$ under different catalyst loadings, as well as a lower HMF yield (up to ca. 66%) and glucose conversion with a higher glucose concentration (1 M). Such limitation is possibly due to the direct contact of the organic phase with some parts of the catalyst bed, inhibiting the sugar transfer and causing degradation of the extracted HMF in mTHF at the prolonged reaction time. Phosphate leaching by hydrolytic cleavage is rather limited and occurred only to a tiny amount of phosphates weakly anchored on the catalyst surface, while the remaining phosphates were strongly incorporated into the framework and robust against leaching. Catalyst deactivation is mainly attributed to the humin accumulation on the acid sites and could be regenerated by a simple re-calcination in air. Compared with the performance in batch and the literature work, significantly enhanced space time yields of HMF (i.e., two orders of magnitude higher) have been achieved in the packed-bed microreactor.

Generally, this work has provided further insights into the relation between the synthesis method, structure, acidic properties and bi-functionality of the in-situ phosphated titania catalysts, and demonstrated a preliminary proof of concept for the combined heterogeneous catalysis, biphasic solvent system and microreactor operation for continuous synthesis of bio-based furanics from cellulosic carbohydrates.

CRediT authorship contribution statement

Wenze Guo: Conceptualization, Validation, Investigation, Data Curation, Writing - Original Draft, Writing - Review & Editing. **Thijn Kortenbach**: Validation, Investigation. **Wei Qi**: Pyridine-IR investigation, Writing - Original Draft. **Emiel Hensen:** XPS investigation, Writing - Review & Editing. **Hero Jan Heeres**: Supervision, Writing - Review & Editing. **Jun Yue**: Conceptualization, Data Curation, Writing - Review & Editing, Supervision, Project administration, Funding acquisition.

Declaration of Competing Interest

The authors declare that they have no known competing financial interests or personal relationships that could have appeared to influence the work reported in this paper.

The authors declare no competing financial interest.

Acknowledgement

This research was financially supported by the University of Groningen (start-up package in the area of green chemistry and technology for Jun Yue). Wenze Guo gratefully acknowledged the financial support from the China Scholarship Council (grant number 201606740069), and the experimental and analytical support from Dr. Wang Yin, Xiang Tang and the technical staff of the Department of Chemical Engineering at the University of Groningen.

Appendix A. Supporting information

Supplementary data associated with this article can be found in the online version at doi:10.1016/j.apcatb.2021.120800.

References

[1] A. Corma, S. Iborra, A. Velty, Chemical routes for the transformation of biomass into chemicals, Chem. Rev. 107 (2007) 2411–2502.
[2] L.T. Mika, E. Cséfalvay, Á. Németh, Catalytic conversion of carbohydrates to initial platform chemicals: chemistry and sustainability, Chem. Rev. 118 (2018) 505–613.
[3] R.-J. van Putten, J.C. van der Waal, E. de Jong, C.B. Rasrendra, H.J. Heeres, J.G. de Vries, Hydroxymethylfurfural, a versatile platform chemical made from renewable resources, Chem. Rev. 113 (2013) 1499–1597.
[4] A.H. Motagamwala, W. Won, C. Sener, D.M. Alonso, C.T. Maravelias, J.A. Dumesic, Toward biomass-derived renewable plastics: production of 2,5-furandicarboxylic acid from fructose, Sci. Adv. 4 (2018) eaap9722.
[5] Y. Román-Leshkov, C.J. Barrett, Z.Y. Liu, J.A. Dumesic, Production of dimethylfuran for liquid fuels from biomass-derived carbohydrates, Nature 447 (2007) 982–985.
[6] S.G. Wettstein, D.M. Alonso, Y. Chong, J.A. Dumesic, Production of levulinic acid and gamma-valerolactone (GVL) from cellulose using GVL as a solvent in biphasic systems, Energy Environ. Sci. 5 (2012) 8199–8203.
[7] A.H. Motagamwala, K. Huang, C.T. Maravelias, J.A. Dumesic, Solvent system for effective near-term production of hydroxymethylfurfural (HMF) with potential for long-term process improvement, Energy Environ. Sci. 12 (2019) 2212–2222.
[8] W. Guo, Z. Zhang, J. Hacking, H.J. Heeres, J. Yue, Selective fructose dehydration to 5-hydroxymethylfurfural from a fructose-glucose mixture over a sulfuric acid catalyst in a biphasic system: experimental study and kinetic modelling, Chem. Eng. J. 409 (2021), 128182.
[9] W. Guo, H.J. Heeres, J. Yue, Continuous synthesis of 5-hydroxymethylfurfural from glucose using a combination of AlCl3 and HCl as catalyst in a biphasic slug flow capillary microreactor, Chem. Eng. J. 381 (2020), 122754.
[10] Y.J. Pagán-Torres, T. Wang, J.M.R. Gallo, B.H. Shanks, J.A. Dumesic, Production of 5-hydroxymethylfurfural from glucose using a combination of Lewis and Brønsted acid catalysts in water in a biphasic reactor with an alkylphenol solvent, ACS Catal. 2 (2012) 930–934.
[11] T. Deng, X. Cui, Y. Qi, Y. Wang, X. Hou, Y. Zhu, Conversion of carbohydrates into 5-hydroxymethylfurfural catalyzed by ZnCl2 in water, Chem. Commun. 48 (2012) 5494–5496.
[12] V. Choudhary, S.H. Mushrif, C. Ho, A. Anderko, V. Nikolakis, N.S. Marinkovic, A. I. Frenkel, S.I. Sandler, D.G. Vlachos, Insights into the interplay of Lewis and Brønsted acid catalysts in glucose and fructose conversion to 5-(hydroxymethyl) furfural and levulinic acid in aqueous media, J. Am. Chem. Soc. 135 (2013) 3997–4006.
[13] A.A. Marianou, C.M. Michailof, A. Pineda, E.F. Iliopoulou, K.S. Triantafyllidis, A. A. Lappas, Effect of Lewis and Brønsted acidity on glucose conversion to 5-HMF and lactic acid in aqueous and organic media, Appl. Catal. A: Gen. 555 (2018) 75–87.
[14] R. Karinen, K. Vilonen, M. Niemelä, Biorefining: heterogeneously catalyzed reactions of carbohydrates for the production of furfural and hydroxymethylfurfural, ChemSusChem 4 (2011) 1002–1016.
[15] Q. Hou, X. Qi, M. Zhen, H. Qian, Y. Nie, C. Bai, S. Zhang, X. Bai, M. Ju, Biorefinery roadmap based on catalytic production and upgrading 5-hydroxymethylfurfural, Green. Chem. 23 (2021) 119–231.
[16] A. Takagaki, M. Ohara, S. Nishimura, K. Ebitani, A one-pot reaction for biorefinery: combination of solid acid and base catalysts for direct production of 5-hydroxymethylfurfural from saccharides, Chem. Commun. (2009) 6276–6278.

[17] M. Ohara, A. Takagaki, S. Nishimura, K. Ebitani, Syntheses of 5-hydroxymethylfurfural and levoglucosan by selective dehydration of glucose using solid acid and base catalysts, Appl. Catal. A: Gen. 383 (2010) 149–155.

[18] C.-H. Kuo, A.S. Poyraz, L. Jin, Y. Meng, L. Pahalagedara, S.-Y. Chen, D.A. Kriz, C. Guild, A. Gudz, S.L. Suib, Heterogeneous acidic TiO2 nanoparticles for efficient conversion of biomass derived carbohydrates, Green. Chem. 16 (2014) 785–791.

[19] L. Jiang, L. Zhou, J. Chao, H. Zhao, T. Lu, Y. Su, X. Yang, J. Xu, Direct catalytic conversion of carbohydrates to methyl levulinate: synergy of solid Brønsted acid and Lewis acid, Appl. Catal., B: Environ. 220 (2018) 589–596.

[20] T.W. Walker, A.K. Chew, H. Li, B. Demir, Z.C. Zhang, G.W. Huber, R.C. Van Lehn, J.A. Dumesic, Universal kinetic solvent effects in acid-catalyzed reactions of biomass-derived oxygenates, Energy Environ. Sci. 11 (2018) 617–628.

[21] Q. Hou, M. Zhen, W. Li, L. Liu, J. Liu, S. Zhang, Y. Nie, C. Bai, X. Bai, M. Ju, Efficient catalytic conversion of glucose into 5-hydroxymethylfurfural by aluminum oxide in ionic liquid, Appl. Catal., B: Environ. 253 (2019) 1–10.

[22] J. Wang, W. Xu, J. Ren, X. Liu, G. Lu, Y. Wang, Efficient catalytic conversion of fructose into hydroxymethylfurfural by a novel carbon-based solid acid, Green. Chem. 13 (2011) 2678–2681.

[23] T. Okuhara, Water-tolerant solid acid catalysts, Chem. Rev. 102 (2002) 3641–3666.

[24] K. Nakajima, Y. Baba, R. Noma, M. Kitano, J.N. Kondo, S. Hayashi, M. Hara, Nb2O5·nH2O as a heterogeneous catalyst with water-tolerant Lewis acid sites, J. Am. Chem. Soc. 133 (2011) 4224–4227.

[25] I. Sádaba, M. López Granados, A. Riisager, E. Taarning, Deactivation of solid catalysts in liquid media: the case of leaching of active sites in biomass conversion reactions, Green. Chem. 17 (2015) 4133–4145.

[26] J. Huo, J.-P. Tessonnier, B.H. Shanks, Improving hydrothermal stability of supported metal catalysts for biomass conversions: a review, ACS Catal. 11 (2021) 5248–5270.

[27] P.J. Fellows. Food Processing Technology: Principles and Practice, Elsevier,, 2009.

[28] Y. Román-Leshkov, J.N. Chheda, J.A. Dumesic, Phase modifiers promote efficient production of hydroxymethylfurfural from fructose, Science 312 (2006) 1933–1937.

[29] J.S. Kruger, V. Nikolakis, D.G. Vlachos, Carbohydrate dehydration using porous catalysts, Curr. Opin. Chem. Eng. 1 (2012) 312–320.

[30] K. Bourikas, C. Kordulis, A. Lycourghiotis, Titanium dioxide (Anatase and Rutile): surface chemistry, liquid–solid interface chemistry, and scientific synthesis of supported catalysts, Chem. Rev. 114 (2014) 9754–9823.

[31] P. Sudarsanam, H. Li, T.V. Sagar, TiO2-based water-tolerant acid catalysis for biomass-based fuels and chemicals, ACS Catal. 10 (2020) 9555–9584.

[32] K. Nakajima, R. Noma, M. Kitano, M. Hara, Titania as an early transition metal oxide with a high density of Lewis acid sites workable in water, J. Phys. Chem. C. 117 (2013) 16028–16033.

[33] R. Noma, K. Nakajima, K. Kamata, M. Kitano, S. Hayashi, M. Hara, Formation of 5-(Hydroxymethyl) furfural by stepwise dehydration over TiO2 with water-tolerant Lewis acid sites, J. Phys. Chem. C. 119 (2015) 17117–17125.

[34] K. Nakajima, R. Noma, M. Kitano, M. Hara, Selective glucose transformation by titania as a heterogeneous Lewis acid catalyst, J. Mol. Catal. A: Chem. 388 (2014) 100–105.

[35] L. Atanda, S. Mukundan, A. Shrotri, Q. Ma, J. Beltramini, Catalytic conversion of glucose to 5-hydroxymethyl-furfural with a phosphated TiO2 catalyst, ChemCatChem 7 (2015) 781–790.

[36] L. Atanda, A. Shrotri, S. Mukundan, Q. Ma, M. Konarova, J. Beltramini, Direct production of 5-hydroxymethylfurfural via catalytic conversion of simple and complex sugars over phosphated TiO2, ChemSusChem 8 (2015) 2907–2916.

[37] W.-Z. Guo, H. Lu, X.-K. Li, G.-P. Cao, Tungsten-promoted titania as solid acid for catalytic hydrolysis of waste bottle PET in supercritical CO2, RSC Adv. 6 (2016) 43171–43184.

[38] X.-K. Li, H. Lu, W.-Z. Guo, G.-P. Cao, H.-L. Liu, Y.-H. Shi, Reaction kinetics and mechanism of catalyzed hydrolysis of waste PET using solid acid catalyst in supercritical CO_2, AlChE J. 61 (2015) 200–214.

[39] G. Li, E.A. Pidko, E.J.M. Hensen, K. Nakajima, A. Density, Functional theory study of the mechanism of direct glucose dehydration to 5-hydroxymethylfurfural on anatase titania, ChemCatChem 10 (2018) 4084–4089.

[40] V.V. Ordomsky, V.L. Sushkevich, J.C. Schouten, J. van der Schaaf, T.A. Nijhuis, Glucose dehydration to 5-hydroxymethylfurfural over phosphate catalysts, J. Catal. 300 (2013) 37–46.

[41] K.T.V. Rao, S. Souzanchi, Z. Yuan, C. Xu, One-pot sol–gel synthesis of a phosphated TiO2 catalyst for conversion of monosaccharide, disaccharides, and polysaccharides to 5-hydroxymethylfurfural, N. J. Chem. 43 (2019) 12483–12493.

[42] O. Martin, N. Bolzli, B. Puértolas, J. Pérez-Ramírez, P. Riedlberger, Preparation of highly active phosphated TiO2 catalysts via continuous sol–gel synthesis in a microreactor, Catal. Sci. Technol. 9 (2019) 4744–4758.

[43] K.J.A. Raj, A.V. Ramaswamy, B. Viswanathan, Surface area, pore size, and particle size engineering of titania with seeding technique and phosphate modification, J. Phys. Chem. C. 113 (2009) 13750–13757.

[44] A.R. Ramadan, N. Yacoub, H. Amin, J. Ragai, The effect of phosphate anions on surface and acidic properties of TiO 2 hydrolyzed from titanium ethoxide, Colloids Surf. A: Physicochem. Eng. Asp. 352 (2009) 118–125.

[45] R. Zheng, L. Lin, J. Xie, Y. Zhu, Y. Xie, State of doped phosphorus and its influence on the physicochemical and photocatalytic properties of P-doped titania, J. Phys. Chem. C. 112 (2008) 15502–15509.

[46] A. Hommes, H.J. Heeres, J. Yue, Catalytic transformation of biomass derivatives to value-added chemicals and fuels in continuous flow microreactors, ChemCatChem 11 (2019) 4671–4708.

[47] M.H. Tucker, A.J. Crisci, B.N. Wigington, N. Phadke, R. Alamillo, J. Zhang, S. L. Scott, J.A. Dumesic, Acid-functionalized SBA-15-type periodic mesoporous organosilicas and their use in the continuous production of 5-hydroxymethylfurfural, ACS Catal. 2 (2012) 1865–1876.

[48] J. Yue, Multiphase flow processing in microreactors combined with heterogeneous catalysis for efficient and sustainable chemical synthesis, Catal. Today 308 (2018) 3–19.

[49] R.M. Abdilla-Santes, W. Guo, P.C.A. Bruijnincx, J. Yue, P.J. Deuss, H.J. Heeres, High-yield 5-hydroxymethylfurfural synthesis from crude sugar beet juice in a biphasic microreactor, ChemSusChem 12 (2019) 4304–4312.

[50] M. Brasholz, K. von Kanel, C.H. Hornung, S. Saubern, J. Tsanaktsidis, Highly efficient dehydration of carbohydrates to 5-(chloromethyl)furfural (CMF), 5-(hydroxymethyl)furfural (HMF) and levulinic acid by biphasic continuous flow processing, Green. Chem. 13 (2011) 1114–1117.

[51] Y. Muranaka, H. Nakagawa, R. Masaki, T. Maki, K. Mae, Continuous 5-hydroxymethylfurfural production from monosaccharides in a microreactor, Ind. Eng. Chem. Res. 56 (2017) 10998–11005.

[52] T. Shimanouchi, Y. Kataoka, T. Tanifuji, Y. Kimura, S. Fujioka, K. Terasaka, Chemical conversion and liquid–liquid extraction of 5-hydroxymethylfurfural from fructose by slug flow microreactor, AlChE J. 62 (2016) 2135–2143.

[53] T.M. Kohl, B. Bizet, P. Kevan, C. Sellwood, J. Tsanaktsidis, C.H. Hornung, Efficient synthesis of 5-(chloromethyl)furfural (CMF) from high fructose corn syrup (HFCS) using continuous flow processing, React. Chem. Eng. 2 (2017) 541–549.

[54] P. Desir, B. Saha, D.G. Vlachos, Ultrafast flow chemistry for the acid-catalyzed conversion of fructose, Energy Environ. Sci. 12 (2019) 2463–2475.

[55] M. Sayed, N. Warlin, C. Hulteberg, I. Munslow, S. Lundmark, O. Pajalic, P. Tunå, B. Zhang, S.-H. Pyo, R. Hatti-Kaul, 5-Hydroxymethylfurfural from fructose: an efficient continuous process in a water-dimethyl carbonate biphasic system with high yield product recovery, Green. Chem. 22 (2020) 5402–5413.

[56] V.V. Ordomsky, J. van der Schaaf, J.C. Schouten, T.A. Nijhuis, Glucose dehydration to 5–hydroxymethylfurfural in a biphasic system over solid acid foams, ChemSusChem 6 (2013) 1697–1707.

[57] J.C. Yu, L. Zhang, Z. Zheng, J. Zhao, Synthesis and characterization of phosphated mesoporous titanium dioxide with high photocatalytic activity, Chem. Mater. 15 (2003) 2280–2286.

[58] L. Körösi, S. Papp, I. Bertóti, I. Dékány, Surface and bulk composition, structure, and photocatalytic activity of phosphate-modified TiO2, Chem. Mater. 19 (2007) 4811–4819.

[59] S.K. Samantaray, K. Parida, Studies on anion-promoted titania: 3. Effect of concentration and source of phosphate ion, method of preparation, and activation temperature on redox, acid–base, textural and catalytic properties of titania, J. Mol. Catal. A: Chem. 176 (2001) 151–163.

[60] K.I. Hadjiivanov, D.G. Klissurski, A.A. Davydov, Study of phosphate-modified TiO2 (anatase), J. Catal. 116 (1989) 498–505.

[61] A.A.S. Alfaya, Y. Gushikem, S.C. de Castro, Highly dispersed phosphate supported in a binary silica−titania matrix: preparation and characterization, Chem. Mater. 10 (1998) 909–913.

[62] J.C. Jacco, The infrared spectra of KTiOPO4 and a K2O·P2O5·TiO2 glass, Mater. Res. Bull. 21 (1986) 1189–1194.

[63] V.N. Sigaev, P. Pernice, A. Aronne, O.V. Akimova, S.Y. Stefanovich, A. Scaglione, KTiOPO4 precipitation from potassium titanium phosphate glasses, producing second harmonic generation, J. Non-Cryst. Solids 292 (2001) 59–69.

[64] A. Bhaumik, S. Inagaki, Mesoporous titanium phosphate molecular sieves with ion-exchange capacity, J. Am. Chem. Soc. 123 (2001) 691–696.

[65] L. Lin, W. Lin, J.L. Xie, Y.X. Zhu, B.Y. Zhao, Y.C. Xie, Photocatalytic properties of phosphor-doped titania nanoparticles, Appl. Catal., B: Environ. 75 (2007) 52–58.

[66] L. Lin, R.Y. Zheng, J.L. Xie, Y.X. Zhu, Y.C. Xie, Synthesis and characterization of phosphor and nitrogen co-doped titania, Appl. Catal., B: Environ. 76 (2007) 196–202.

[67] M.A. Arillo, M.L. López, C. Pico, M.L. Veiga, A. Jiménez-López, E. Rodríguez-Castellón, Surface characterisation of spinels with Ti(IV) distributed in tetrahedral and octahedral sites, J. Alloy. Compd. 317–318 (2001) 160–163.

[68] S. Guo, S. Han, M. Haifeng, C. Zeng, Y. Sun, B. Chi, J. Pu, J. Li, Synthesis of phosphorus-doped titania with mesoporous structure and excellent photocatalytic activity, Mater. Res. Bull. 48 (2013) 3032–3036.

[69] S.M. Mukhopadhayay, S.H. Garofalini, Surface studies of TiO2·SiO2 glasses by X-ray photoelectron spectroscopy, J. Non-Cryst. Solids 126 (1990) 202–208.

[70] S.J. Splinter, R. Rofagha, N.S. McIntyre, U. Erb, XPS characterization of the corrosion films formed on nanocrystalline Ni–P alloys in sulphuric acid, Surf. Interface Anal. 24 (1996) 181–186.

[71] S. Baunack, S. Oswald, D. Scharnweber, Depth distribution and bonding states of phosphorus implanted in titanium investigated by AES, XPS and SIMS, Surf. Interface Anal. 26 (1998) 471–479.

[72] A.S. Poyraz, C.-H. Kuo, E. Kim, Y. Meng, M.S. Seraji, S.L. Suib, Tungsten-promoted mesoporous group 4 (Ti, Zr, and Hf) transition-metal oxides for room-temperature solvent-free acetalization and ketalization reactions, Chem. Mater. 26 (2014) 2803–2813.

[73] R. Weingarten, Y.T. Kim, G.A. Tompsett, A. Fernández, K.S. Han, E.W. Hagaman, W.C. Conner, J.A. Dumesic, G.W. Huber, Conversion of glucose into levulinic acid with solid metal(IV) phosphate catalysts, J. Catal. 304 (2013) 123–134.

[74] Y. Román-Leshkov, M. Moliner, J.A. Labinger, M.E. Davis, Mechanism of glucose isomerization using a solid Lewis acid catalyst in water, Angew. Chem. Int. Ed. 49 (2010) 8954–8957.

[75] A. Hommes, A.J. ter Horst, M. Koeslag, H.J. Heeres, J. Yue, Experimental and modeling studies on the Ru/C catalyzed levulinic acid hydrogenation to γ-valerolactone in packed bed microreactors, Chem. Eng. J. 399 (2020), 125750.

[76] Z. Cao, Z. Fan, Y. Chen, M. Li, T. Shen, C. Zhu, H. Ying, Efficient preparation of 5-hydroxymethylfurfural from cellulose in a biphasic system over hafnyl phosphates, Appl. Catal., B: Environ. 244 (2019) 170–177.
[77] M.I. Alam, S. De, B. Singh, B. Saha, M.M. Abu-Omar, Titanium hydrogenphosphate: an efficient dual acidic catalyst for 5-hydroxymethylfurfural (HMF) production, Appl. Catal. A: Gen. 486 (2014) 42–48.
[78] A. Dutta, A.K. Patra, S. Dutta, B. Saha, A. Bhaumik, Hierarchically porous titanium phosphate nanoparticles: an efficient solid acid catalyst for microwave assisted conversion of biomass and carbohydrates into 5-hydroxymethylfurfural, J. Mater. Chem. 22 (2012) 14094–14100.
[79] A. Visan, R.G.H. Lammertink, Fructose dehydration to hydroxyl-methylfurfural in an immobilized catalytic microreactor, J. Flow. Chem. 10 (2020) 461–468.
[80] A.-K. Liedtke, F. Scheiff, F. Bornette, R. Philippe, D.W. Agar, C. de Bellefon, Liquid–solid mass transfer for microchannel suspension catalysis in gas–liquid and liquid–liquid segmented flow, Ind. Eng. Chem. Res. 54 (2015) 4699–4708.
[81] L.J. Konwar, P. Mäki-Arvela, J.-P. Mikkola, SO3H-Containing functional carbon materials: synthesis, structure, and acid catalysis, Chem. Rev. 119 (2019) 11576–11630.